(*Pt/MWCNT*) AND (*Pt/f-MWCNT*) CATALYSTS PREPARATION BY HYDROGEN REDUCTION AND IMPREGNATION METHOD: THE APPLICATION TO METHANOL OXIDATION REACTION

A THESIS SUBMITTED TO
THE GRADUATE SCHOOL OF NATURAL AND APPLIED SCIENCES
OF
MIDDLE EAST TECHNICAL UNIVERSITY

BY

MOHAMMED AHMED M. ZABARA

IN PARTIAL FULFILLMENT OF THE REQUIREMENTS
FOR
THE DEGREE OF MASTER OF SCIENCE
IN
CHEMISTRY

SEPTEMBER 2016

Approval of the thesis:

Pt/MWCNT and Pt/f-MWCNT Catalysts Preparation by Hydrogen Reduction and Impregnation Method: The Application to Methanol Oxidation Reaction

Submitted by **Mohammed Ahmed M. Zabara** in partial fulfillment of the requirements for the degree of **Master of Science in Chemistry Department, Middle East Technical University** by,

Prof. Dr. Gülbin Dural Ünver
Dean, Graduate School of **Natural and Applied Sciences** _____

Prof. Dr. Cihangir Tanyeli
Head of Department, **Chemistry** _____

Prof. Dr. Gülsün Gökağaç
Supervisor, **Chemistry Dept., METU** _____

Examining Committee Members:

Prof. Dr. Saim Özkar
Chemistry Dept., METU _____

Prof. Dr. Gülsün Gökağaç
Chemistry Dept., METU _____

Prof. Dr. Mürvet Volkan
Chemistry Dept., METU _____

Assoc. Prof. Dr. Metin Aydın
Chemistry Dept., OMU _____

Assoc. Prof. Dr. Emren Nalbant Esentürk
Chemistry Dept., METU _____

Date: 06/09/2016

I hereby declare that all information in this document has been obtained and presented in accordance with academic rules and ethical conduct. I also declare that, as required by these rules and conduct, I have fully cited and referenced all materials and results that are not original to this work.

Name, Last name: Mohammed Ahmed M. Zabara

Signature:

ABSTRACT

Pt/MWCNT and Pt/f-MWCNT Catalysts Preparation by Hydrogen Reduction and Impregnation Method: The Application to Methanol Oxidation Reaction

Mohammed Ahmed M. Zabara
M. Sc., Department of Chemistry
Supervisor: Prof. Dr. Gülsün Gökağaç

September 2016, 92 pages

In this thesis, multi-walled carbon nanotubes supported platinum nanoparticles (Pt/MWCNT) and functionalized multi-walled carbon nanotubes supported platinum nanoparticles (Pt/f-MWCNT) catalysts in different Pt percentages were prepared using impregnation method and hydrogen gas reduction. Firstly, multi-walled carbon nanotubes were functionalized using sonochemical method and characterized by Fourier transform infra-red spectroscopy (FTIR), X-ray photoelectron spectroscopy (XPS), and acid base back titration. Secondly, Pt/MWCNT and Pt/f-MWCNT were prepared and characterized by X-ray diffraction (XRD), transmission electron microscopy (TEM), X-ray photoelectron spectroscopy (XPS), and inductively coupled plasma mass spectrometry (ICP-MS). Their electrochemical properties and performance toward methanol oxidation reaction were examined by cyclic voltammetry (CV).

FTIR and XPS studies showed the formation of carboxylic acid, carbonyl, and hydroxyl groups on the surface of f-MWCNT. XRD and TEM works indicated the formation of faced center cubic structure platinum nanoparticles for all catalysts and the average particle size of Pt nanoparticles were little larger for Pt/f-MWCNT (~3nm) than Pt/MWCNT (~2nm) when only the nanoparticles were considered. Agglomeration of Pt nanoparticles was detected for Pt/MWCNT, while narrow particle size distribution was noticed for Pt/f-MWCNT which specifies the positive effect of

the functional groups on MWCNT. XPS data revealed three oxidation states of platinum, 0, +2 and +4, with a percentage of ~ 65, 20 and 15, respectively. CV analysis displayed that 14 wt% Pt/f-MWCNT has the highest performance toward methanol oxidation reaction, which is 4.8 times more than commercial E-TEK Pt/Vulcan XC-72 catalyst, because it has the highest electrochemical surface area (72.30 m^2/g), percent Pt utility (70.9%), and roughness factor (134.9) compared to other catalysts.

Keywords: Direct Methanol Fuel Cell, multi-walled carbon nanotubes, supported platinum nanoparticles, impregnation method.

ÖZ

Hidrojen İndirgeyici ve İmpregnasyon Yöntemi Kullanarak Pt/MWCNT ve Pt/f-MWCNT Katalizörler Hazırlaması: Metanol Yükseltgeme Tepkimesinde Uygulaması

Mohammed Ahmed M. Zabara
Yüksek Lisans, Kimya Bölümü
Tez Yöneticisi: Prof. Dr. Gülsün Gökağaç

Eylül 2016, 92 sayfa

Bu tezde, hidrojen gazıyla indirgeme ve impregnasyon yöntemi kullanılarak çok duvarlı karbon nanotüp ile desteklenen platin nanoparçacıklar (Pt/MWCNT) ve fonksiyonlaştırılmış karbon nanotüp ile desteklenen platin nanoparçacıklar (Pt/f-MWCNT) hazırlanmıştır. Öncelik, sonokimyasal metod kullanarak çok duvarlı karbon nanotüpler fonksyonlandırılmış ve Fourier kızılötesi spektroskopi (FTIR), X-ışını foto elektron spektroskopisi (XPS) ve asit-baz titrasyonu kullanılarak karakterize edilmiştir. Daha sonra, Pt/MWCNT ve Pt/f-MWCNT hazırlanmış ve X-ışını kırınımı (XRD), geçirgen elektron mikroskobu (TEM) ve X-ışını foto elektron spektroskopi (XPS) ve İndüktif olarak bağlanmış plazma spektrometre (ICP-MS) kullanarak karakterize edilmiştir. Bunların elektrokimyasal özellikleri ve metanol yükseltgeme tepkimesine karşı performansları dönüşümlü voltametre (CV) ile tanımlanmıştır.

FTIR ve XPS sonuçları, f-MWCNT üzerinde karboksilik asit, karbonil, ve hidroksil grupların oluştuğunu göstermiştir. XRD ve TEM çalışmaları tüm katalizör için Pt nanoparçacıklar yüzey merkezli kübik yapıya sahip olduğunu ve sadece nanoparçacıklar göz önüne alındığında Pt/f-MWCNT katalizördeki Pt nanoparçacıklarının (~3nm) Pt/MWCNT'de bulunan nanoparçacıklarından (~2nm) biraz daha büyük olduğunu göstermiştir. Pt/MWCNT'de Pt nanoparçacıklarında

topaklanma gözlemlenirken Pt/f-MWCNT'de dar parçacık büyüklüğü dağılımı gözlenmiş ve bu da MWCNT'deki fonksiyon gruplarının olumlu etkisini sergilemiştir. XPS verileri, platinin üç yükseltgenme halinin, Pt(0) ~ 65%, Pt(II) ~ 20 ve Pt(IV) ~ 15%, olduğunu ortaya koymuştur. Yüksek elektrokimyasal yüzey alanına (72.30 g / m2), Pt kullanımına (% 70.9) ve pürüzlülük faktörü (134.9) sahip olan 14 ağ.% Pt.f-MWCNT'ün metanol yükseltgenme tepkimesine karşı en yüksek performansa sahip olduğu ve bunun da ticari E-TEK Pt/Vulcan XC-72 katalizörden 4.8 kat daha fazla olduğu bulunmuştur.

Anahtar Kelimeler: Doğrudan Metanol Yakıt Pili, karbon nanotüpler, desteklenen platin nanopartiküller, emdirme yöntemi.

To my family

ACKNOWLEDGEMENTS

Firstly, I would like to express my sincere appreciation and thanks to my supervisor Prof. Dr. Gülsün Gökağaç for her guidance, encouragement, support and valuable ideas throughout the research.

I would like to thank Prof. Dr. Ayşen Yılmaz for her help during XRD measurement.

I want to thank my lab-mates Gerçem and Seda for their help during my study.

I wish to express my special thanks to my dearest friends Yusuf Samet Aytekin, Muzaffer Gencay Çelik, and Metehan Severoğlu for their help, encouragement, and fruitful discussions during my research work.

I would like to express my gratitude to the defense committee members for the useful comments on this thesis.

I am also thankful to the staff of METU Central Laboratory for their help during TEM, XPS, and ICP-MS characterization analyses.

Finally, I would like to thank my family for their support and encouragement during the writing of this thesis.

TABLE OF CONTENTS

LIST OF TABLES

TABLES

LIST OF FIGURES

FIGURES

CHAPTER 1

INTRODUCTION

The demand for clean and more efficient technologies for electric energy production is in continuous growth. This growth is due to the environmental concerns and the depletion of the non-renewable energy sources. Endless research are done to develop systems and technologies that can replace the non-renewable sources. Several solutions were introduced and some are still under development. These solutions include the usage of different renewable energy sources such as solar energy, and wind energy. Another solutions include the usage of new systems such as fuel cell which depend on clean fuels such as hydrogen and methanol.

Fuel cell technology is one of the promising solutions that were introduced for the clean energy production issue. Fuel cells display excellent potential as a clean source for electric energy with very low amounts of hazardous gas emission and high efficiencies. Fuel cells are considered as the 21st century technology for clean energy [1]. They are applied in different applications now days. These applications include transportation, stationary, and portable electronic devices. Yet there are challenges that prevents fuel cells from the integration in our daily life use. These challenges varies from the structure of fuel cells, reactions in its compartments, and fuel storage and transportation.

The Direct Methanol Fuel Cell (DMFC) is one type of fuel cells which exhibits high interests. It has promising potential due to its low operating temperature, high energy density, and absence of storage and transportation problems for methanol [2]. However, DMFC needs development in its structure materials and methanol oxidation

reaction activity. Oxidation of methanol is very slow and a catalyst is needed to activate the oxidation reaction. The development of active catalyst is one of the important issues in the development of DMFC. For this purpose the fuel cells, and DMFC will be briefly described in this chapter and then a literature review related to the development of a catalyst for methanol oxidation using nanotechnology will be presented in the next chapter.

1.1 Fuel Cells

Fuel cells are energy conversion systems. They are electrochemical devices which directly convert chemical energy in fuels into electric energy. This conversion is obtained through oxidation reduction (redox) reaction [3]. The electrochemical process that takes place in the fuel cell can convert up to 80% of the chemical energy [1]. On the other hand, conventional methods of energy conversion can convert up to 40% of the chemical energy of the fuel [1]. This is due to the thermodynamic and mechanical limitation of the process.

Conventional methods of producing electric energy such as internal combustion engine include intermediate steps. The steps for the production of electrical energy include:

- Combustion of fuels for the conversion of chemical energy into heat.
- Conversion of heat into mechanical energy using heat engine.
- Conversion of the mechanical energy into electricity by generator.

Fuel cells eliminate these steps and converts directly the chemical energy into electric energy by one electrochemical reaction. Figure 1.1 illustrates the difference between the fuel cell and the heat engine for producing electricity. The combustion step releases huge amount of CO, SO_x, NO_x, and other harmful gases. In the case of fuel cells the only waste product from the electrochemical process is water for hydrogen fuel cells

and low amounts of carbon dioxide for methanol fuel cells. This makes the fuel cells one of the cleanest devices for the production of electric energy [4]. The other conversion steps require the presence of moving parts which decreases the conversion efficiency of the method. In the case of the fuel cells, elimination of these parts simplify the structure and removes the sound pollution that is produced from these steps.

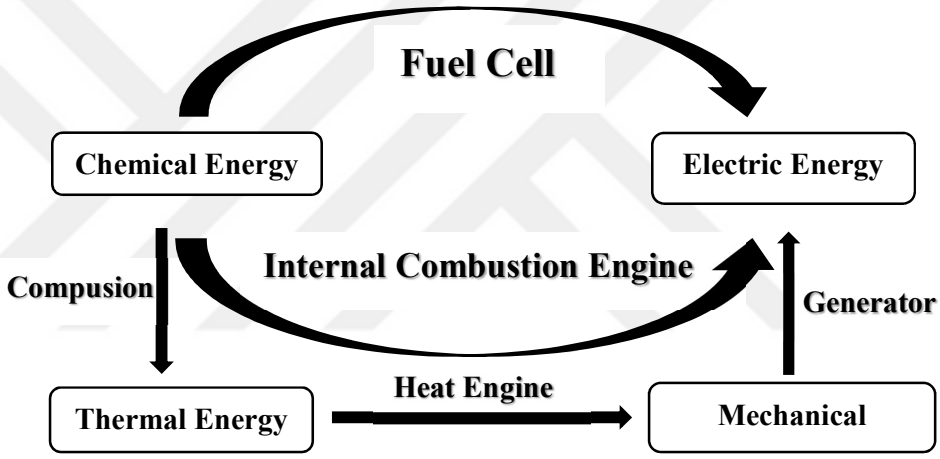

Figure 1.1. Difference between fuel cell and internal combustion engine for electric energy production

Beside the consideration of fuel cells as electric energy production systems, they are also considered as electric energy storage systems. Electric energy storage systems such as batteries are electrochemical cells in which their working principle like fuel cells is based on the conversion of the chemical energy to electrical energy by redox reaction. However, the difference between batteries and fuel cells is in the locations of

energy storage and conversion [4]. Batteries are closed systems where the energy conversion and storage happen in the same compartments. Though, fuel cells are open systems where the energy conversion takes its place in the reaction compartments and the storage of the fuel is in other compartments of the cell such as tank. In other words, the storage of the electric energy in the fuel cells are in the form of fuels, whereas it is stored in the batteries in the form of electric energy.

Fuel cells have the advantage over batteries by providing the electric energy continuously as long as the fuel is provided to them. Batteries in other hand can only store the electric energy by charging. When they are discharged the electric energy should be stored again through charging process. This makes batteries reliable to other sources for electricity whereas fuel cells rely on the supplement of the fuels for the production of electricity.

The mentioned properties and advantages of the fuel cells make them ideal systems for clean energy production. However, there are also some disadvantages of fuel cells that limits their usage in our daily lives. These disadvantages are related to the chemicals used in the system, durability of materials, and the cost of the technology. Points of advantages and disadvantages of fuel cell are summed in Table 1.1 [4]. The complexity of fuel cells is related to the substances that are used in their operation. The electrochemical process in fuel cells requires highly active catalysts, and special polymeric membranes. These complex materials need special synthesis methods and increase the cost of the technology. Furthermore, the durability of the existed materials is still low and further research and development should be done to improve them [5].

Moreover, there are some issues which are related to the structure of fuel cells and the reactions in their compartments. These issues have high impact in reducing the performance of the fuel cells. Overcoming these problems is one of the important research fields in the way of improving fuel cell technology. The solutions introduced are represented in finding new materials such as catalysts and membranes which are used in the compartments of the fuel cell. These new materials enhance the efficiency

of the reactions and improve the performance of fuel cells [3]. Further discussion of theses point will be done in the following chapters considering working principles and structure.

Table 2.1 Advantages and disadvantages of fuel cells [4]

Advantages
Efficient energy conversion
Almost nonpolluting
Silent
Safe
High energy density
Disadvantages
Complex to operate
Low durability
Expensive
Low power density per volume

1.1.1 Brief History of Fuel Cells

Although fuel cells have been known to be the future technology for electric energy production, they are one of the oldest devices for energy conversion. Fuel cells have been developing since the eighteenth century. This development was not displayed in

the market except for the last decades due to the discovery of the combustion engine which showed wide applications for humans needs [6].

It all started by the discovery of the field of electrochemistry by Luigi Galvani in 1791. He noticed the movement of the frog's leg when attached to the tip of scalpel. This movement was caused when the metal attached the nerves causing the muscle to contract. He called this phenomenon animal electricity. In 1800 Alessandro Volta found that it was not the frog's leg that produced the electricity. The movement was just an indicator of the electricity caused by the different metals attached to the frog's legs. Volta developed his first voltaic pile by placing a membrane in contact with two metallic plates of silver and zinc and witting it in salt water. An electric current was obtained in the external circuit when the two plates were connected. This was the first conversion of chemical energy into electric energy which lead to the discovery of batteries and fuel cells [7].

The principles of the fuel cells were introduced by Sir William Robert Grove in 1839. It was discovered accidently when he was preforming an electrolysis experiment that current was flowing in the opposite direction when the battery is disconnected from the electrolyzer and the two electrodes are connected together. The current was flowing in opposite direction with the consumption of the gases hydrogen and oxygen found in the electrolyzer. He called his discovery gas battery which produced a cell potential of 1V. His gas battery consisted of platinum electrodes placed in test tubes of hydrogen and oxygen immersed in a bath of dilute sulfuric acid which is shown in Figure 1.2. His invention opened a door in new discoveries in the field of fuel cells [7].

The term fuel cell was firstly introduced by Charles Langer and Ludwig Mond in 1889. They worked on Grove's electrochemical cell (gas battery) and developed the first fuel cell. After that in 1893, Friedrich Wilhelm Ostwald who is the founder of the field physical chemistry experimentally explained the connection of various components of a fuel cell: electrodes, electrolyte, oxidizing and reducing agents, anions and cations. This helped in the understanding of the fuel cell operation and its development [8].

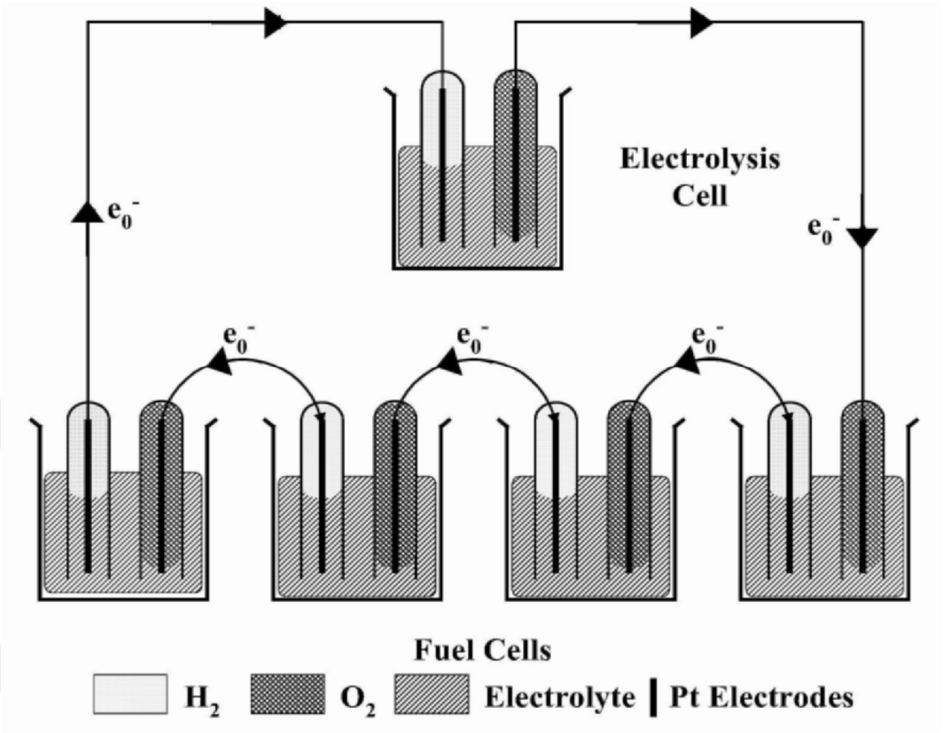

Figure 1.2. Grooves gas battery [7]

By moving to the twentieth century, William W. Jacques and Emil Baur leading researchers in the field of fuel cells made big contributions in fuel cell technology. In 1921, Baur built the first molten carbonate fuel cell. At the same time Jacques was the first one to build high power systems of fuel cells: a 1.5-kW fuel cell with a stack of 100 tubular units, and a fuel cell of 30 kW [8].

Following that in 1933 Thomas Francis Bacon a chemical engineer at the University of Cambridge developed the first practical fuel cell made of hydrogen and oxygen. In 1959, with the support of the company Marshall Aerospace, Bacon presented a fuel cell of 40 cells of 5 kW and 60% efficiency [8].

In 1955, Thomas Grubb, a chemist who worked for General Electric Company (GE), modified the original design of the fuel cell. He introduced different ion exchange membrane one of them is polystyrene sulfated ion exchange membrane. Another scientist in GE Company named Leonard Niedrach introduced a way of depositing platinum on the membrane which acts as a catalyst for the reactions at the compartments. Following these developments in fuel cell technology NASA started the use of fuel cells in its space missions in 1960 [9].

In 1990 a new type of fuel cell was introduced that used methanol rather than hydrogen as a fuel. This type of fuel cell was called Direct Methanol Fuel Cell. It was invented by the Jet Propulsion Laboratory of NASA in conjunction with the University of Southern California. This type of fuel cell showed many advantages that is related to the liquid fuel methanol and its operating temperature 50 - 80 °C [9].

In the 21st century few applications of fuel cells started to involve in our daily life. Some of these applications include the introduction of automobiles that operate on fuel cells, and primitive electrical charging devices that used fuel cell to produce electric energy. Yet these applications are still limited due to the high cost and the low efficiency of the produced fuel cells. Figure 3 shows the timeline of the important contributions in the history of the fuel cell from origin until present day [10].

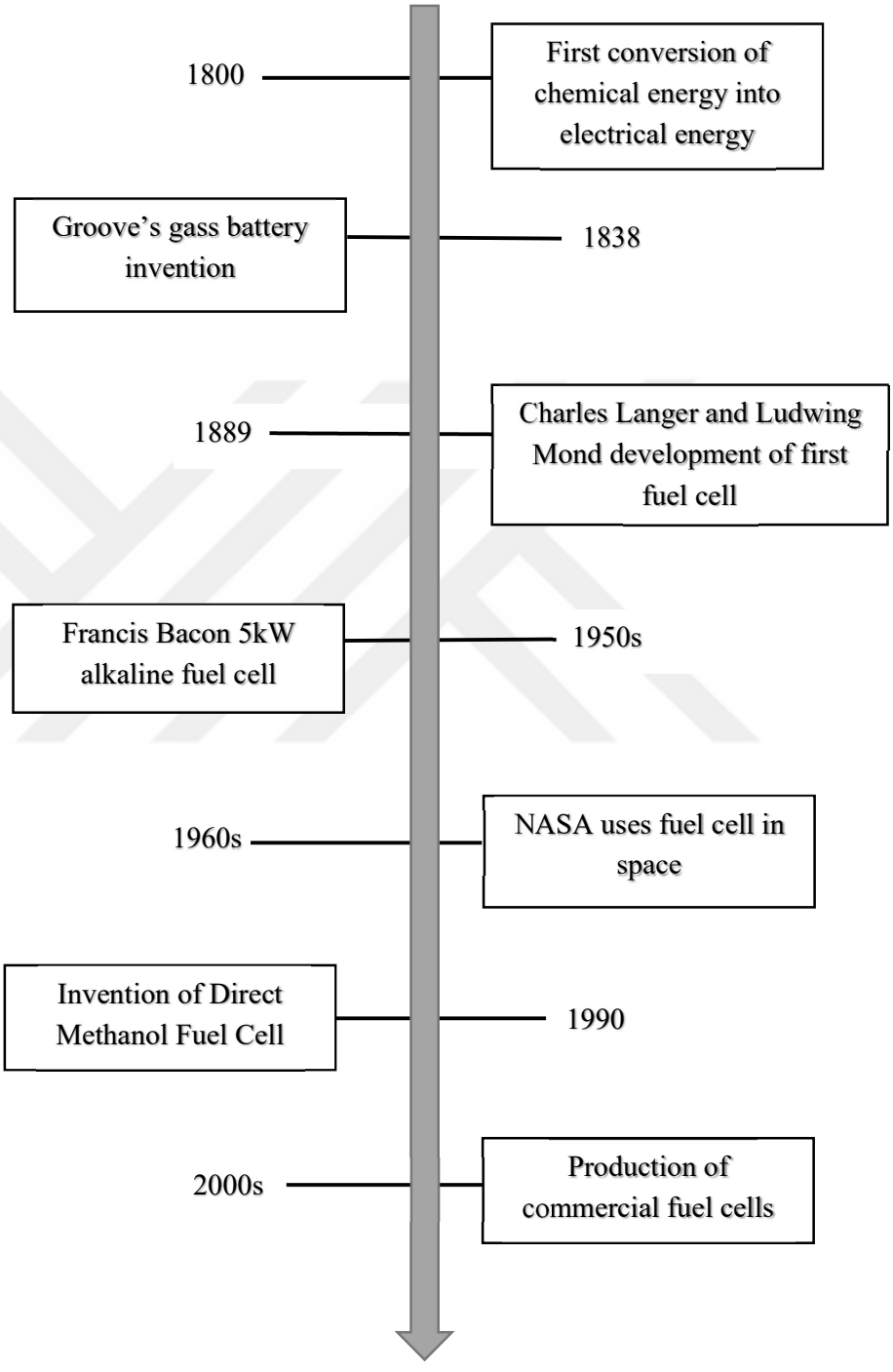

Figure 1.3. Timeline of important contributions in fuel cell history

1.1.2 Principles of Fuel Cells

The working principle of fuel cells depends on the conversion of the chemical energy of fuels directly into electric energy in one step. This one step conversion is based on electrochemical oxidation reduction (redox) reaction. The redox reaction is exhibited in terms of cell potential and electrical current output [11]. The thermodynamics and efficiency of the redox reaction is discussed in this section.

1.1.2.1 Thermodynamics

The fuel cell reaction is a chemical process separated into two electrochemical half-cell reactions. The overall reaction can be described as:

$$a_{ox1} + b_{red1} \rightarrow c_{red2} + d_{ox2}$$

The voltage of the fuel cell is expressed by the difference between the reduction and the oxidation half-cell reactions, which is expressed as ΔE. In fuel cell the free chemical energy is converted to electrical energy. The expression of the Gibbs free energy change is related to the cell voltage by the following equation:

$$\Delta G = -nF\Delta E$$

Where, (n) is the number of electrons involved in the reaction, (F) is the Faraday's constant, and (ΔE) is the difference of the reaction potential. The oxidation reaction is either the direct oxidation of hydrogen or methanol, while the reduction reaction is oxygen reduction mostly from air.

However, the cell voltage of the fuel cell is not ideal and it is less than the theoretical value. The losses in voltage are due to the over potential and the resistance that comes from the electrolyte plus the kinetics differences between the oxidation and reduction reactions [12].

1.1.2.2 Efficiency

The thermal efficiency of an energy conversion system is defined as the amount of useful energy produced relative to the change in stored chemical energy which is released when a fuel is reacted with an oxidant and is expressed by the following equation [9]:

$$\varepsilon = \frac{\Delta G}{\Delta H}$$

Where ΔG is the Gibbs free energy change during the operation of the fuel cell and ΔH is the enthalpy of formation which is the amount of the energy released when burning the fuel. For some types of fuel cells, the efficiency can reach up to 80% which is high compared to heat engines which can reach up to 40%.

The direct conversion of the energy that takes its place in fuel cells is different than the conventional conversion systems which was mentioned previously. The efficiency calculations also varies due to that difference. For fuel cell systems the efficiency is better calculated as electrochemical efficiency rather than thermal efficiency. Electrochemical efficiency is used to compare between different designs and components of fuel cells. The electrochemical efficiency is calculated by the following equation:

$$\varepsilon_{el} = \frac{-nFE}{\Delta G}$$

The electrochemical efficiency gives better understanding when comparing different types of fuel cells because it is directly related to the performance of the fuel cell [12].

1.1.3 Structure of fuel cells

Fuel cells as an electrochemical cell consist of three main parts; anode, cathode and electrolyte. The anode compartment is where the oxidation reaction takes place. The fuel is consumed in the anode forming electrons, reductants (charge carriers), and waste in the form of heat and water in hydrogen fuel cell and carbon dioxide in methanol fuel cells. The electrons are transferred in closed circuit toward the cathode while the reductants are transferred to the cathode through the electrolyte. In the cathode, the reduction reaction takes its place. The reductants that were transferred from the anode are reduced by combining with oxidants mostly oxygen from air.

The electrolyte of the fuel cell depends on the type of the fuel cell used. The electrolyte transfers the reductants and connects the anode to cathode. Figure 1.4 shows the structure of conventional fuel cell.

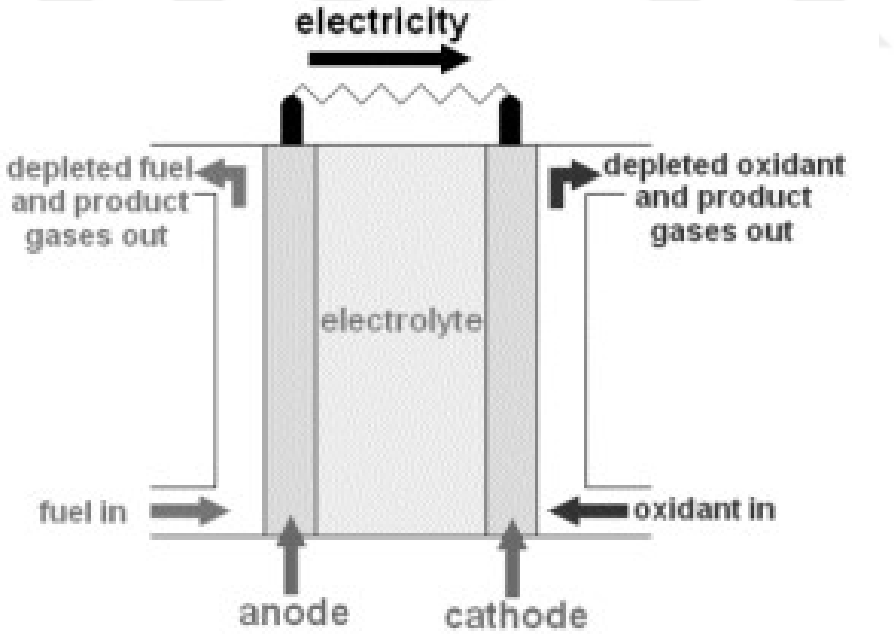

Figure 1.4. Structure of fuel cells [1]

1.14 Types of Fuel Cells

Fuel cells can be classified according to different categories depending on the combination of type of fuel and oxidant, the type of electrolyte, or the temperature of operation [12]. The most common classification is according to their electrolytes. This classification categorizes fuel cells into five types which are:

- Polymer electrolyte membrane fuel cell (PEMFC)
- Alkaline fuel cell (AFC)
- Phosphoric acid fuel cell (PAFC)
- Molten carbonate fuel cell (MCFC)
- Solid oxide fuel cell (SOFC)

The operating temperature also plays an important role in the classification of the fuel cell because the physical state of the electrolyte is determined by the operating temperature. The low temperature fuel cells have aqueous electrolytes and they are used in most practical applications. The fuels used in these fuel cells are hydrogen and alcohols such as methanol. In high temperature fuel cells, fuels such as carbonate and methane can be used because of the rapid electrode kinetics caused by the high temperature. The electrolyte used in these high temperature fuel cells are solids such as, nonporous metal oxides and ceramic matrix [13].

The direct methanol fuel cell (DMFC) belongs to the proton electrolyte membrane fuel cell (PEMFC). However, instead of hydrogen gas, which is used as fuel in a PEMFC, the DMFC uses methanol aqueous solution as the fuel feeding the anode. DMFCs using liquid methanol fuel have been considered to be a favorable option in terms of fuel usage and feed strategies. Types of fuel cells are listed in table 1.2 with electrolyte classification and operating temperature.

Table 1.2. Types of fuel cells [13]

	Polymer electrolyte membrane fuel cell (PEMFC)	**Alkaline fuel cell (AFC)**	**Phosphoric acid fuel cell (PAFC)**	**Molten carbonate fuel cell (MCFC)**	**Solid oxide fuel cell (SOFC)**
Electrolyte	Ion Exchange Membranes	Mobilized or Immobilized Potassium Hydroxide	Immobilized Liquid Phosphoric Acid	Immobilized Liquid Molten Carbonate	Ceramic
Operating Temperature	25-80°C	65°C-220°C	205°C	650°C	600-1000°C
Charge Carrier	H^+	OH^-	H^+	CO_3^{2-}	O^{2-}
Prime Cell Components	Carbon-based	Carbon-based	Graphite-based	Stainless based	Ceramic
Catalyst	Platinum	Platinum	Platinum	Nickel	Perovskites

1.1.5 Applications of Fuel cells

The applications of fuel cells vary according to the type and the usage area of the fuel cell. Restrictions to their usage are related to the working temperature, efficiency and performance of the cell. Fuel cells can be used in stationary, transportation, and in portable applications. The range of power of fuel cells starts from 1 Watt to 10 Mega Watts. This big range enables fuel cells to have diverse applications [8]. Some of these applications are:

- Stationary applications: Fuel cell systems can be installed for hospitals, hotels, offices and schools. These systems are connected to the grid to provide more electrical power to the facilities. This helps in reducing the consumption of the local grid electric power. In other case, they can be installed for independent facilities in isolated areas to provide them with the electric power. Melton Carbonate and Solid Oxide fuel cells are the most used for stationary applications. These fuel cells operate at high temperatures which enables them to generate heat power as well as electric power. This co-generation can increase the efficiency up to 85% while reducing energy consumption.

- Applications for transportation: Vehicle producers are currently using fuel cell vehicles for research, development or testing. These vehicles helps in reducing CO_2 emissions and noise contaminations. Some examples of these vehicles are now available in markets under testing. They use Polymer Exchange Membrane fuel cells which use hydrogen as a fuel. These fuel cells have zero CO_2 emission if the hydrogen is produced from renewable sources. Another type of applications for transportation is the usage of fuel cells in in electrical conveyor machinery and forklifts. The use of fuel cells in these machines reduces the cost and the environmental toxic impact. The cost is reduced due to the reduction of the maintenance and replacements in the fuel cell systems which have no moving parts. Plus the continuous supply of the electric power with no need for charging [14].

- Portable applications: Fuel cell can provide electric power where local grid is not available in areas such as camping. They can replace the diesel engine and prevent the harmful emissions and noises. Also they are used as supporting units when the grid power is shut down in emergency situations.

- Micro power applications: In electronic devices, batteries are used as electricity source which require charging in each use. The usage of fuel cells in electronics will increase their battery lives. Companies such as Motorola, Toshiba, Samsung, Panasonic, Sanyo and Sony have developed some examples of fuel cells that can power telecommunication devices and laptops. The choice for the type of fuel cell in these application is Direct Methanol fuel cell. DMFC can provide electric power up to 100 Watts with liquid fuel methanol which is stable at room temperature.

Fuel cells have wide and promising applications, yet efficiencies of the used fuel cells need to increase in order to reduce the cost of the used technology. Table 1.3 shows the range of applications for different types of fuel cells.

Table 1.3. Range of applications of fuel cells [3]

Applications	Portable and electronic devices			Transportation			Power generations	
Power in Watts	1	10	100	1k	10k	100k	1M	10M
Types of fuel cell	DMFC			AFC			MCFC	
	PEMFC					SOFC		

1.2 Direct Methanol Fuel Cell

DMFC, as mentioned before, was invented by the Jet Propulsion Laboratory of NASA in conjunction with the University of Southern California in 1990. It is classified as PEMFCs since polymer membrane is used as electrolyte and protons as charge carriers.

DMFCs use a liquid fuel methanol which has many advantages over hydrogen or other fuels such as methane. First, the liquid state of methanol in ambient temperatures makes it suitable for portable devices and transportation applications. Liquid state facilitate the storage of the fuel and increase the safety of the cell. Second, the energy density of methanol is one of the highest densities among other fuels which can be seen in figure 1.5. Third, methanol can be produced by renewable energy sources such as wood, agricultural wastes, and other biomass resources by thermochemical processes [15].

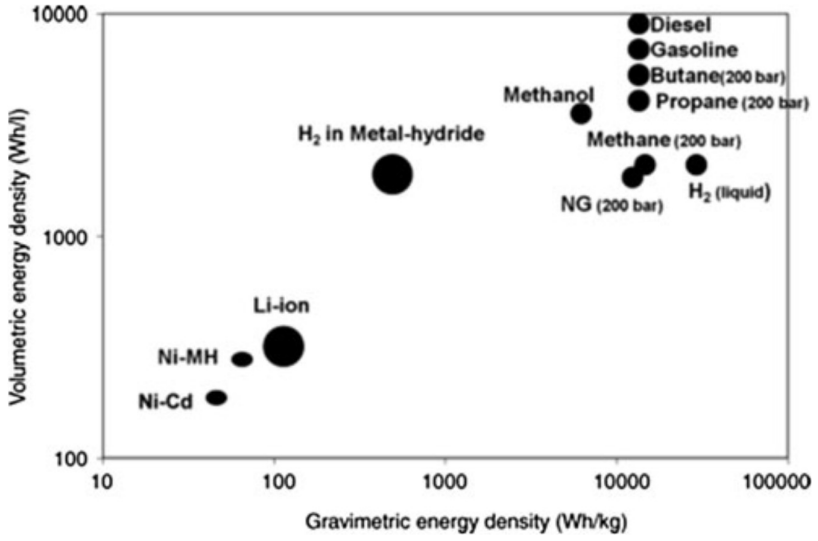

Figure 1.5. Gravimetric and volumetric energy density of many fuels and batteries [14]

These attractive properties of methanol in terms of its energy density, ease of distribution, and potential for production from renewable sources make the DMFC the best choice among the fuel cells for transportation, portable, and electronic applications. However, there are some issues that constrain the usage of DMFC in today's market. These issues include the high cost, low efficiency, and durability of the DMFC which need to be developed. These problems are related to the structure and construction materials of DMFC. Improving the structure materials will result in the improvement of its performance [14].

1.2.1 Working Principle and Structure

Figure 1.6 illustrates the structure of the DMFC. It consists of the anode where the oxidation of the methanol achieves. The cathode where the reduction of oxygen from air takes place. The electrolyte membrane where the charge carrier (protons) are transferred from the anode to the cathode.

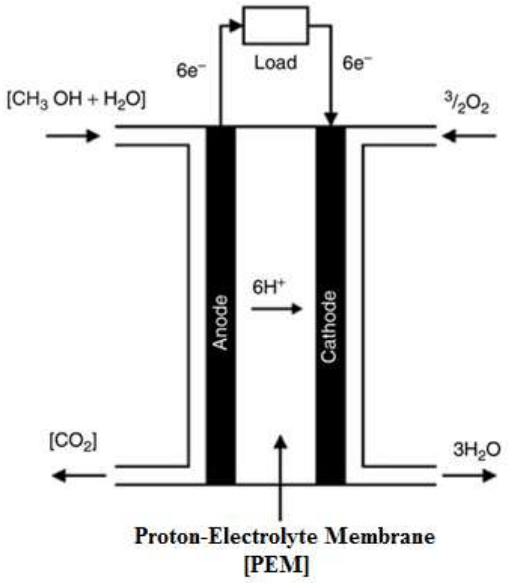

Figure 1.6. Structure of DMFC [14]

The anode, cathode, and overall redox reaction process that take place in DMFC are shown below:

- Anode reaction:

$$CH_3OH + H_2O \rightarrow CO_2 + 6H^+ + 6e^-$$

- Cathode reaction:

$$3/2\,O_2 + 6H^+ + 6e^- \rightarrow 3H_2O$$

- Overall reaction:

$$CH_3OH + 3/2\,O_2 \rightarrow CO_2 + 2H_2O$$

One molecule of the fuel methanol is oxidized to release six electrons, six protons and a carbon dioxide molecule. The electrons are carried to outer circuit while the protons are transferred to the cathode through the electrolyte membrane. In the cathode oxygen is reduced to water with the help of the transferred protons and electrons.

The free energy change, ΔG, associated with the overall redox reaction as mentioned before is directly related to the reversible cell potential ΔE via:

$$\Delta G = -nF\Delta E$$

Where n is the number of electrons involved in the chemical reaction (n = 6 electrons per mole of methanol), F is the Faraday's constant (96,485 coulombs per mole), and ΔE is the equilibrium reversible cell potential which is at 25 °C and 1atm is 1.18V [16]. As a result the free energy change at the same condition is:

$$\Delta G = -683\ kJ\ mol^{-1}$$

1.2.2 Limitations with Methanol Oxidation

The simple structure and thermodynamic properties of the DMFC show excellent operation conditions. Though, there are mainly three problems that need to be solved in order to reach the high operation conditions. First problem is related to the electrolyte membrane of the DMFC. There is a methanol crossover the membrane which cause the decrease in the overall efficiency of the cell. Second problem is the slow kinetics of the oxidation reaction of methanol which cause an over potential for the cell. Lastly, the diffusion of the liquid fuel methanol at the surface of the anodic layer represents another issue [17]. The limitation regarding the electro-catalyst to activate the methanol reaction is the only limitation to be discussed in this study.

Thermodynamically from the values listed before, oxidation of methanol should be favorable due to the high methanol oxidation free energy. However, the methanol oxidation kinetics is very slow at low temperatures (<80 °C). As a result there is a need for a catalyst to speed up the reaction. The best catalyst that shows the highest activity for the methanol oxidation is platinum. However, even with the best platinum catalyst the methanol oxidation reaction is still slow and cause an over potential of about 250mV [18].

Moreover, the oxidation reaction of methanol is not one step reaction and it involves many intermediates. Some of the intermediates are irreversible and are adsorbed at the surface of the catalyst. Figure 1.7 shows the proposed mechanism for the oxidation of methanol with the present of the Pt catalyst [19]. From the mechanism it can be noticed that there is a parallel reaction pattern that takes place for water adsorption and methanol adsorption. Both of these pathways require a Pt catalyst which should be able to dissociate the C-H bond and to facilitate the reaction of the resulting residue with some O-containing species such as HO_{ads} and H_2O_{ads} to form CO_2. However, the resulting residues do not always react with O-containing species resulting in the formation of CO which acts as poison for the catalyst.

This necessitate the Pt catalyst to have high surface area and high activity for water activation and C-H bond activation. A catalyst with these properties will reduce the CO poisoning effect and increase the activity of the methanol oxidation.

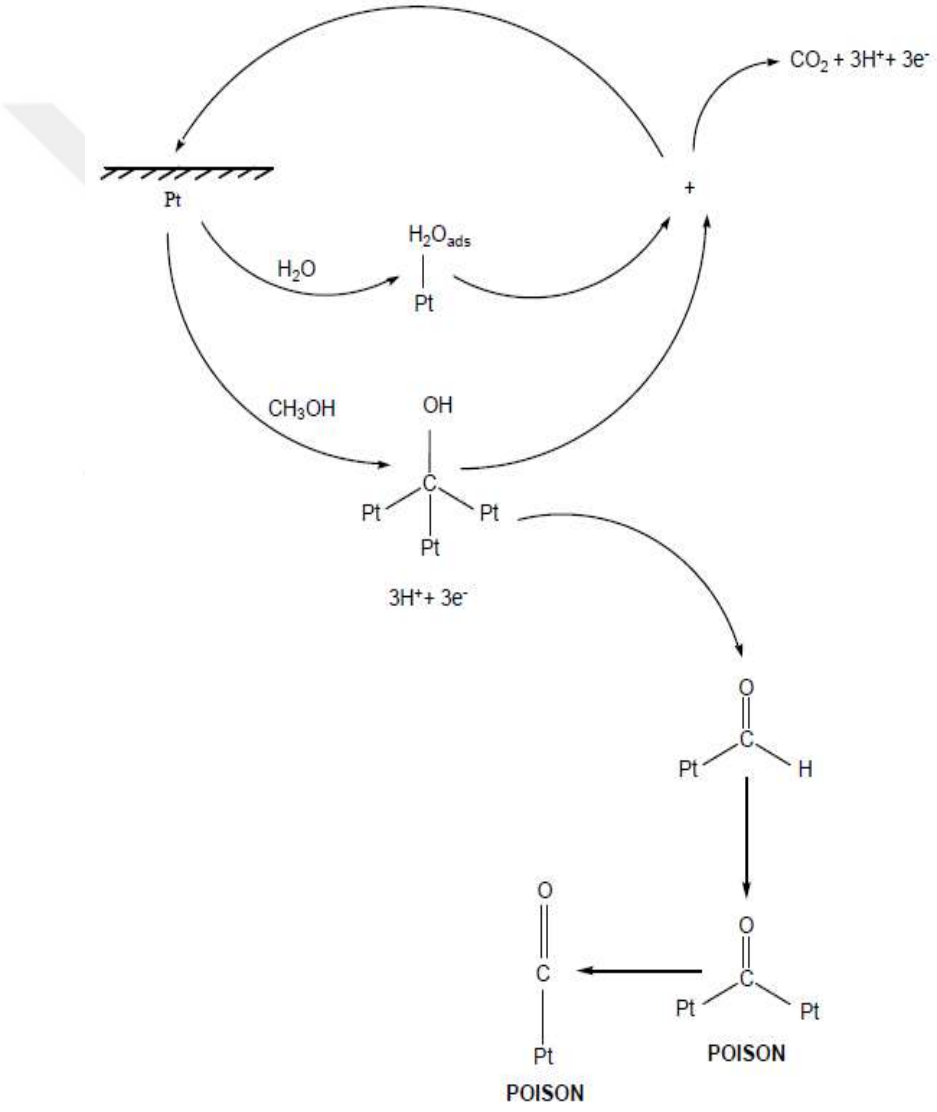

Figure 1.7. Proposed mechanism for methanol oxidation reaction [19]

1.2.3 Electro-Catalyst Development for DMFC

The best electro-catalyst that can activate the oxidation of methanol is known to be the carbon supported platinum catalyst. The practical electro-catalyst for DMFC applications must have the following properties [18]:

- High intrinsic activity for higher current density at DMFC operating voltage.
- Excellent electro-chemical stability.
- Easy scale-up for low manufacturing cost.
- Low cost with less Pt content on a carbon support.
- Good ink formulation with desirable viscosity, particle size and hydrophilic/hydrophobic properties which to fit the membrane manufacturing process.

Since the invention of DMFC, many research have been done to develop electro-catalysts with the described properties. Carbon supported Pt catalysts are prepared with different methods and then an ink is made out of this supported catalyst. The supporting strategy aims at getting a stable dispersion of the electro-catalyst over the support and at reducing the loading of Pt [20].

The catalytic activity of the supported Pt catalysts was found to be affected by the size of the Pt particles. The size changes effect the local electronic structure of the catalyst (electronic effects) and also the availability of sites on its surface (geometric effects). Decreasing the particle size of Pt results in better catalytic activity due to the high surface area to mass ratio [20]. For this reason many studies have been done to develop Pt-nanoparticles that can be supported onto different carbon supports. The next chapter will discuss the theory behind the Pt nanoparticles electro-catalysts preparation and will review the literature works that were done in the preparation of the Pt nanoparticle electro catalysts for fuel cells.

CHAPTER 2

LITERATURE REVIEW

2.1 Pt nanoparticles Based Catalyst for DMFC

Electro-catalysis for DMFC requires the use of Pt metal nanoparticles with high electroactive surface area. The studies related to the effect of size variation on the efficiency of methanol oxidation reaction suggest that Pt nanoparticles with the size range 3-10 nm show the maximum mass specific activity [20]. The narrow size distribution of the nanoparticles is also significant for the high activity of the catalyst. This is due to the similar interactions among the oxidation products with the same sized nanoparticles. Large size difference between the particles leads to different interactions among the oxidation products causing a decrease in the activity of the catalyst [20].

The size effect depend on the preparation method of the Pt nanoparticles and the kind of support used in the catalyst. The preparation method for the supported nanoparticle should produce Pt nanoparticles with controlled and narrow size distribution over the support. Furthermore, the support must have high surface area, good morphology, and high conducting ability. The supports used in the preparation of DMFC catalyst are carbon based supports such as active carbon, carbon black, single and multi-walled carbon nanotubes. The preparation methods for the Pt nanoparticles are following the bottom-up approach starting with platinum precursor as the starting material [21].

There are three main methods for the preparation of carbon supported Pt nanoparticles catalyst. These methods are impregnation method, colloidal method, and micro emulsion method [21]. All of the three methods include a chemical step for the

formation of the nanoparticles from the precursor and a deposition step for the dispersion of the nanoparticles over the support. Figure 2.1 summarize the steps of the mentioned methods.

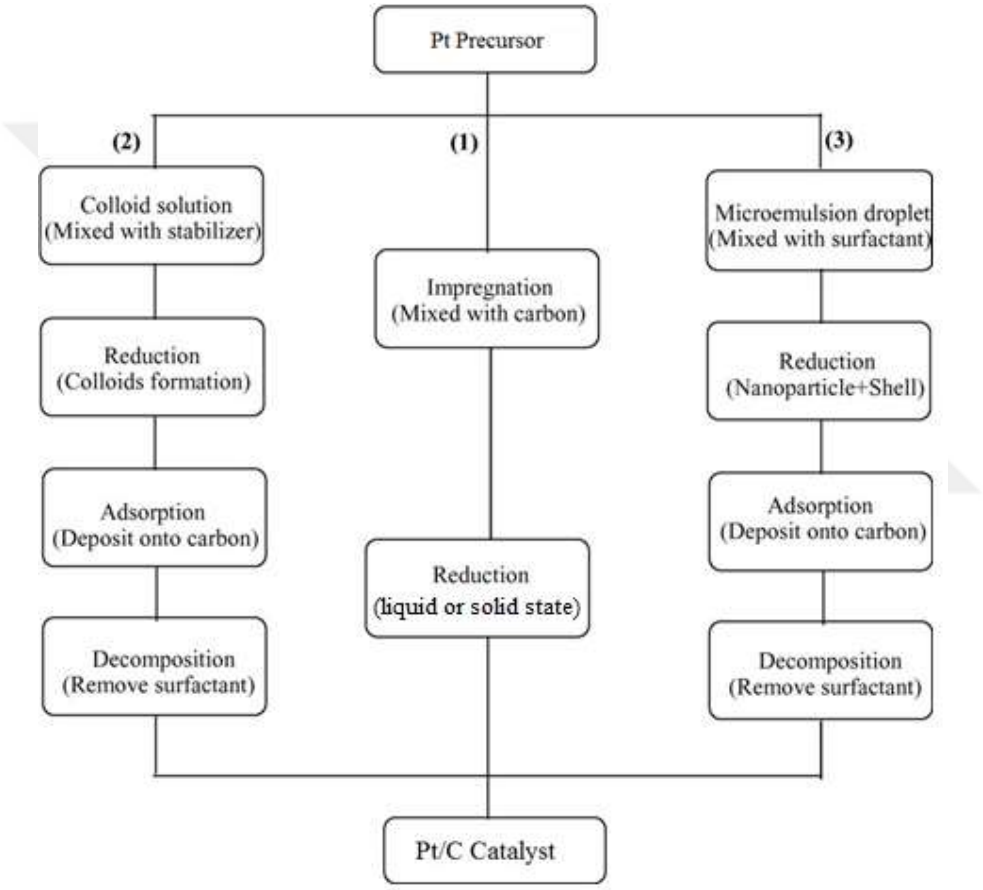

Figure 2.1. Preparation methods for Pt/C catalysts: (1) The impregnation method, (2) the colloidal method and (3) the micro emulsion method [21]

We can notice from figure 2.1 the differences among the three methods in the formation step of the nanoparticles and their deposition on the support. In the

impregnation method the precursor is directly mixed with the carbon support. In the other methods a surfactants or stabilizers are used in the step before the formation of the nanoparticles. Surfactants and stabilizers work in control the particle size of the formed nanoparticles in the reduction step. However, there is a need for the removal of these materials after the formation of the nanoparticles. The removal of these materials does not happen completely and some of them stay at the surface of the nanoparticles which reduce the surface activity of the catalyst. Impregnation method has advantage over the other methods for not using surfactants or stabilizers. Yet, in impregnation method care must be taken in the reduction step to control the size of the formed nanoparticles which is very hard especially in liquid states [20].

The reduction is the step where the formation of the nanoparticles takes place. The precursor which is a platinum complex is reduced into metallic platinum nanoparticles. The reduction step can be done with different reducing agents and in different reduction conditions. The critical point of the reduction step is to form Pt nanoparticles with controlled particle size and to avoid the agglomeration of these nanoparticles. In impregnation method reduction is done for the mixture of the precursor and the support. The formation of the nanoparticles is happening on the surface of the support. While in the other methods formation of the nanoparticles occur in surfactant solution then the formed nanoparticles are deposited on the support. This is also another advantage for the impregnation method where the deposition step is eliminated [22].

The impregnation method shows advantages over the other methods in reducing the number of steps and not using surfactants. These advantages must be taken into consideration in the synthesis of Pt nanoparticle catalyst for DMFC. Though, in impregnation methods many factors can affect the size and the morphology of the nanoparticles such as the type of the reducing agent, type of the support, and the reduction conditions. These factors must be controlled by adjusting the conditions, using suitable reducing agent, and choosing proper support.

In this study the impregnation method is chosen as the preparation method for the supported Pt nanoparticle due to the mentioned advantages. The detailed process of the method will be discussed in the following sections. Additionally, the required support must have high surface area and help in the formation of the nanoparticles. For these reasons, multi-walled carbon nanotubes are used as the support for our catalyst preparation. The properties of the carbon nanotubes will be discussed in the next section.

2.2 Carbon Nanotubes

Carbon nanotubes (CNT) were firstly observed more than two decades ago, in 1990, by the Japanese scientist Iijima. This observation was a few years after the discovery of fullerenes in the mid of 1980s. Fullerenes are geometric cage-like structures of carbon atoms which are composed of hexagonal and pentagonal faces. On the other hand CNT are long cylinder fullerenes where the walls of the tubes are hexagonal carbon covalently bonded to each other (graphite structure) [23].

CNT show extraordinary properties due to their honeycomb symmetric structure. These properties include mechanical, electrical, and thermal properties. For example, reported studies stated strengths that is 10–100 times higher than the strongest steel at a fraction of the weight, thermal conductivity about twice as high as diamond, and electric current carrying capacity 1000 times higher than copper wires [23]. These properties made CNT one of the most investigated materials for the last two decades. Many research also have been done to use CNT as a support for Pt nanoparticles in DMFC catalyst. CNT have large surface areas 300-1300 m^2/g [24] which makes them suitable for catalysis applications where surface area plays an important role in the activity of the catalyst.

2.2.1 Structure of CNT

Carbon nanotubes can be visualized as a sheet of graphite that has been rolled into a tube. The properties of the CNT depends mainly on three factors. First, the atomic arrangement of the carbon atoms which is dependent on the way of the rolling of the graphite sheet shown in Figure 2.2. Second, the length of the tube which is determined by the synthesis method. Third, the morphology or the nanostructure of the tubes.

The rolling of the graphite sheet can be done in three different forms which is shown in figure 2.2. The resulted CNT can have armchair, zigzag, or chiral form. There are three main synthesis methods for CNT which are arc discharge, laser ablation, and chemical vapor deposition. These synthesis methods will not be discussed here but can be seen in reference [25]. The length of the CNT can range from few nanometers to tenth of micrometers while the diameter of the tubes can be in few nanometer scale.

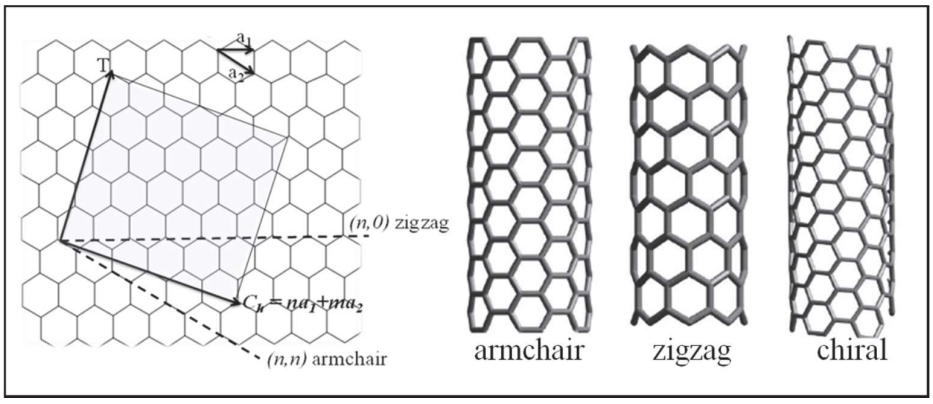

Figure 2.2. A sheet of graphene rolled to show formation of different types of single walled carbon nanotube [25].

There are basically two types of CNTs: single-walled carbon nanotubes (SWCNT) and multi-walled carbon nanotubes (MWCNT). SWCNT represent the fundamental cylindrical structure, whereas MWCNT are formed from interlayer of the cylindrical structure of the rolled graphite layers shown in Figure 2.3.

Both of these types are used in catalysis applications. Platinum nanoparticles are deposited at the surface of the CNTs. After that an ink is made out of the supported catalyst and used in the manufacturing of the electrolyte membrane for DMFC. However, CNT are made of covalently bonded carbon atoms with sp^2 hybridization, as a result the surface of CNT is rather inert and deposition of the Pt nanoparticles with narrow size distribution is challenging process. Furthermore, this inertness increase the difficulty of making ink out of these supported catalyst.

The solution for this problem is the introduction of active groups on the surface of the CNT by a method called functionalization. These groups helps in the narrow distribution of the nanoparticles and in ink preparation. Functionalization of the CNT is discussed in the next section.

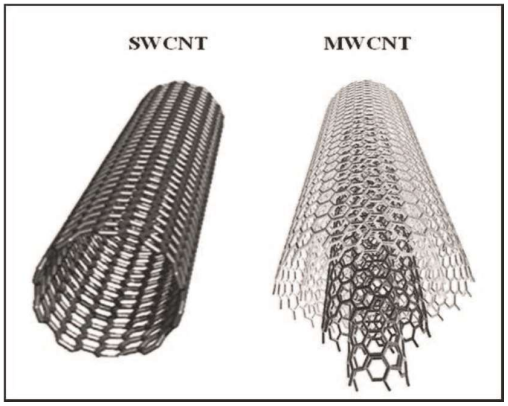

Figure 2.3. Single-walled and Multi-walled carbon nanotubes [25]

2.2.2 Functionalization of CNT

The addition of different functional groups to the surface or the edge of the CNT is called functionalization of the CNT. These functional groups can be oxygen containing groups such as carbonyl, hydroxyl and carboxyl groups. Functionalization of CNT is a chemical process that can be done sonochemically, thermally, electrochemically, and photochemically. Due to the stable structure of the CNT, functionalization is a tough chemical process and requires the treatment of CNT with strong reactants in hard conditions [26].

One of the significant methods that was developed for the functionalization of the CNT involves the extensive ultrasonic treatment in a concentrated mixture of nitric and sulfuric acids. This method is called sonochemical treatment of CNT and result in the oxidation of the CNT to form oxygen containing groups at the surface and the edges. The drastic conditions in this treatment cause the opening of the caps of CNT and the formation of holes or defects at the walls of CNT followed by oxidative etching along the walls. The products of such treatment are CNT fragments with length at the range of 100-300 nm, whose edges and sidewalls are decorated with oxygen containing groups [27].

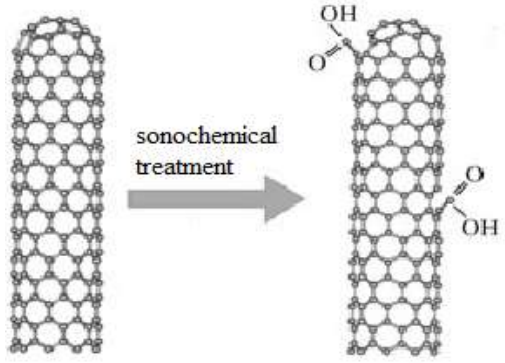

Figure 2.4. Sonochemical treatment of CNT [27]

In this study, the sonochemical method is followed for the functionalization of the CNT with oxygen containing groups. These groups play important role in the deposition of the Pt nanoparticles in the formation of the electro catalyst for DMFC.

2.3 CNT Supported Platinum Nanoparticles for DMFC

CNT represent one of the best support materials for Pt supported electro-catalyst preparation. This is due to its morphology, specific surface area, and high conductivity. The deposition of the Pt nanoparticles on CNT can be done by impregnation method which was mentioned previously.

As was stated, impregnation method have two steps. First step include the mixing of the precursor and the support CNT to form a homogenous mixture in which the precursor is well dispersed over the support. This can be achieved using direct mixing or ultra-sonication. Second step is the reduction step where chemical reduction is done to convert the precursor into Pt nanoparticles over the support. This step is very important step since the Pt nanoparticles tend to agglomerate and form big particles. Choosing the proper reducing agent and the best conditions for reduction is the key to synthesize high quality nanoparticles for impregnation method.

To overcome the challenges related to the reduction step, the reduction is done by thermal reduction under the hydrogen atmosphere in which the mixture of the precursor and CNT are in solid state. This reduces the agglomeration problem and result in the formation of well distributed nanoparticles. This method was firstly mentioned in the literature by the study done by Bin Xue et al. in 2001 where they synthesized different metallic nanoparticles over the CNT. The average particle size of the synthesized Pt nanoparticles was 8 nm with an acceptable size distribution. The result of this study show the applicability of the method in the formation of Pt nanoparticles under 10 nm for electro-catalysis of methanol oxidation reaction.

However, enhancement of the synthesis conditions and the materials should be done to achieve smaller size plus better size distribution [28].

Other studies were published for the synthesis of the Pt nanoparticles using the same procedure but with different supports such as carbon black, carbon xerogels, and multi-walled carbon nanotubes [29-31]. One study which is done by V. Sara Thoi et al. published in 2015 stated the synthesis of CNT supported Pt nanoparticles with average size of 9.4 nm. These nanoparticles were used for solid acid electrochemical cells and not for DMFC [32].

In another study that was published in 2004 by Yangchuan Xing, functionalized CNT supported Pt nanoparticles were synthesized with small average particle size of less than 5 nm and narrow size distribution. The synthesis method used was different from the impregnation method, nevertheless the functional CNT acted as better support for the formation of the Pt nanoparticles. The synthesized nanoparticles were tested for the cathode of polymer electrolyte membrane (PEM) fuel cells [33]. Other results show the same enhancement of the size and the size distribution for the nanoparticles formed on the functionalized CNT [34]. Such studies implies the importance of the introduction of functional groups to the surface of the CNT for better formation of the nanoparticles. In this study, impregnation method was used for the preparation of both MWCNT and functionalized-MWCNT supported Pt nanoparticles.

2.4 Aim of the Study

Production of electrical energy by environment-friendly and highly efficient methods is one of the big challenges for humankind. DMFC offers promising potential for such clean, safe, and efficient energy production. However, issues regarding electrolyte membrane and electro-catalyst need to be solved. In this study, electro-catalyst point has been considered. For this purpose, MWCNT and f-MWCNT supported Pt nanoparticles were prepared by impregnation and hydrogen reduction method to obtain

better catalyst for methanol oxidation reaction. The catalysts were characterized by FTIR, XPS, XRD, TEM and ICP-MS. Electrochemical characterization and the activity toward methanol oxidation reaction of the catalysts were determined by CV.

CHAPTER 3

EXPERIMENTAL

3.1 Chemicals

H_2SO_4 (95-97%, Merck), HNO_3 (65%, Merk), MWCNT (99% R : 9.5nm, L : 10µm, Nanografi), NaOH (99%, Merck), HCl (fuming 37%, Merck), $NaHCO_3$ (99%, Merck), H_2PtCl_6 (Sigma-Aldrich), CH_3CH_2OH (99.9%, Merck), CH_3OH (99.8%, Merck), CCl_4 (99%, Merck), $HClO_4$ (60%, Merck), nafion (5%, Sigma-Aldrich), dimethylformamide (Merck), N-Methyl-2-pyrrolidone (Merck) were used without any purification. Deionized water (18 MΩ) was obtained by Millipore water purification system.

3.2 Functionalization of CNT

The MWCNT were functionalized by sonochemical treatment in strong acidic solution. Ultrasound waves assisted the oxidation of the sp^2 carbon atoms by strong acids. Procedure was taken from the literature with some adjustments [35, 36]. In a typical functionalization procedure, 100 mg of MWCNT were immersed in 60 ml acidic solution (1:3 conc.HNO_3 to conc.H_2SO_4). To reduce the agglomeration of the MWCNT during sonication, the MWCNT acid mixture was stirred for five minutes after sonication for other five minutes. This step was repeated three times and it was then put into sonication bath (Transsonic T700) for 8 hours. After sonication, 250 ml of deionized water was added dropwise with mixing and it was left overnight without mixing. The mixture was vacuum filtrated (0.20µm cellulose nitrate filter paper) and

washed with copious amounts of de-ionized water until pH ≈ 5 was reached. The functionalized-MWCNT were collected and put into oven at 100 °C until the evaporation of all water. The dried f-MWCNT were ready for characterization and Pt-nanoparticles deposition.

3.3 Characterization of the f-MWCNT

Qualitative and quantitative characterization of f-MWCNT were performed to determine the composition and the amount of the functional groups that were introduced. The qualitative analysis was performed by Fourier Transform Infra-Red Spectroscopy (FTIR) and X-ray Photoelectron Spectroscopy (XPS). Spectra in the mid infrared region of 400-4000 cm^{-1} were measured for both MWCNT and f-MWCNT in FTIR. XPS spectra were also obtained between 50 – 550 eV. Quantitative characterization was achieved using acid-base back titration. Moreover, The XPS analysis also gave us information about the relative quantity of the elements found at the surface of the f-MWCNT.

3.3.1 Fourier Transform Infra-Red Spectroscopy (FTIR)

Fourier Transform Infra-Red spectroscopy is straightforward technique for the determination of the presence of C-C, C-O, C-H and others. In infrared spectroscopy, IR radiation is passed through a sample. Some of the infrared radiation is absorbed by the sample and some of it is passed through (transmitted). The resulting spectrum represents the molecular absorption and transmission, creating a molecular fingerprint of the sample [37]. Figure 3.1 shows the diagram of the FTIR instrument.

In this study, KBr was used as the reference material and the solid samples of MWCNT and f-MWCNT were mixed with KBr for pellets preparation. FTIR spectra were measured by Bruker 66 v/s by using KBr pellets with 15 scans at room temperature in METU chemistry department.

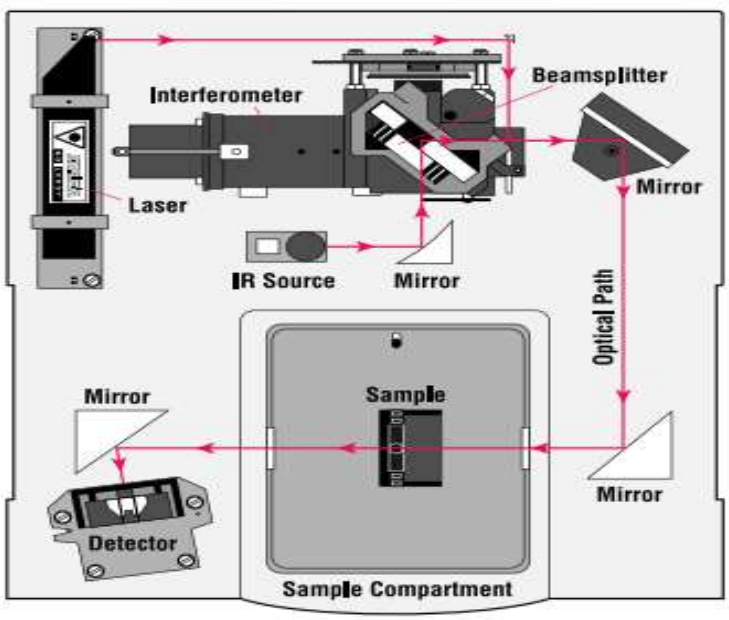

Figure 3.1. FTIR instrument [37]

3.3.2 X-ray Photoelectron Spectroscopy (XPS)

In electron spectroscopy the emission and energy analysis of low energy electrons in the range 20 - 2000 eV is investigated. These electrons are emitted from the samples being examined as a result of the photoemission process. An electron spectrometer consists of a source of primary radiation, and an electron energy analyzer in which all are contained in a vacuum chamber. The source of X-ray photoelectron spectroscopy

is soft X-rays, generally Al Ka or Mg Ka [38]. The structure of the XPS instrument is shown in the Figure 3.2.

In XPS an electron is ejected from a core level by an X-ray photon. The energy of the emitted photoelectrons is then analyzed by the electron spectrometer. The data is presented as a graph of intensity versus electron energy in eV. Once a photoelectron has been emitted, the ionized atom is relaxed. This can be achieved by the emission of an X-ray photon. The other possibility is the ejection of an Auger electron [39]. This auger electrons cause the appearance of peaks in the spectrum which can give information about the samples. Figure 3.3 shows the mechanism of the ejection and the relaxation of the electrons.

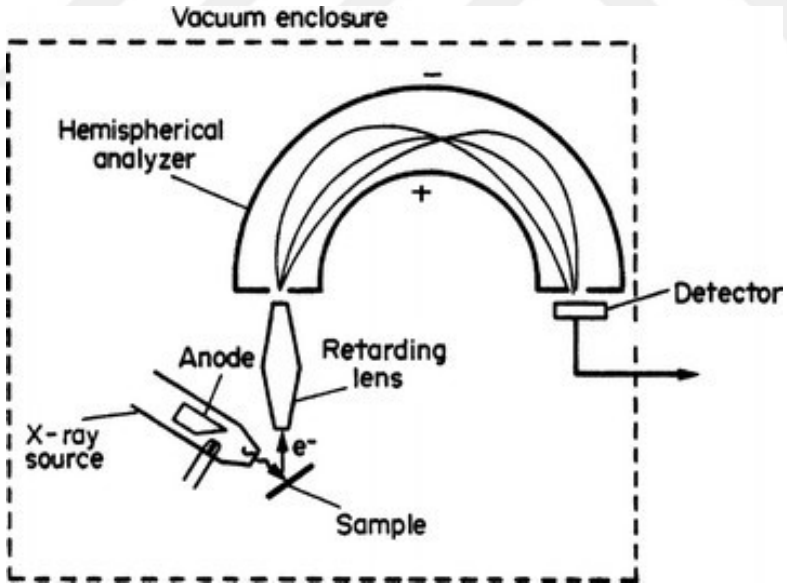

Figure 3.2. XPS instrument [39]

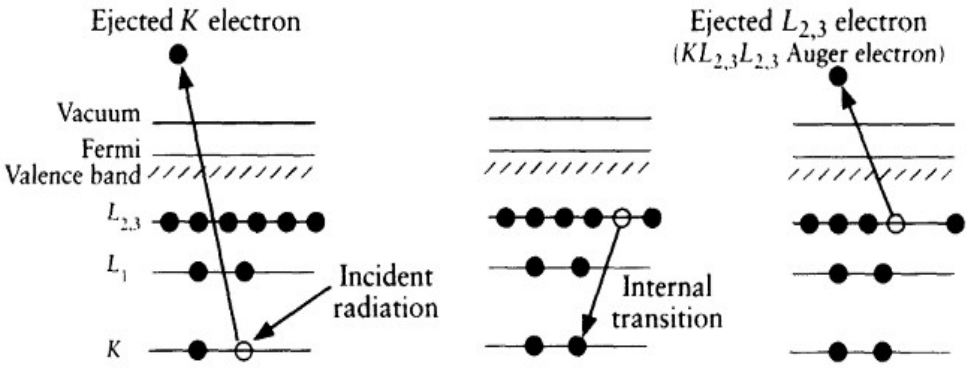

Figure 3.3. Mechanism of the ejection and the relaxation of the electrons [39]

Specs Spectrometer instrument was used for XPS analysis (Central Lab., METU) and Kα lines of Mg (1253.6 eV, 10 mA) were utilized as an X-ray source.

3.3.3 Acid-Base Back Titration

Acid base titration is a widely used method for the determination of the acidic and basic character of many materials. The titration of the f-MWCNT with NaOH and $NaHCO_3$ determines the quantity of the acidic sites in f-MWCNTs. The sodium ions in NaOH are exchanged with protons of the acidic sites while in $NaHCO_3$ are exchange with protons of carboxylic acid sites in f-MWCNT. Determination of the exchanged sodium ions allow us to determine the amount of acidic sites in f-MWCNT [36]. The titration procedure can be shown by the following reactions:

$$MWCNT - COOH\ or\ COH\ +\ NaOH\ or\ NaHCO_3(excess) \rightarrow MWCNT - COO - Na^+\ or\ CO{-}Na^+ + NaOH(determined\ by\ titration)$$

The procedure followed in the titration experiment was taken from the literature [40]. Direct acid base titration was done by stirring 50 mg of f-MWCNT in 50 ml 0.05 M NaOH for 48 h under nitrogen atmosphere. Prolonged stirring was required for the f-MWCNT to equilibrate with the basic solution. The mixture was then filtered and washed with small amount of de-ionized water using 0.20 μm cellulose nitrate filter paper. The combined filtrate and the washings were collected and 50 ml of 0.05 M HCl was added and boiled for 20 min. After cooling to room temperature, the excess HCl was titrated with 0.05 M of NaOH to reach the natural point (pH 7.00), as monitored by a pH meter. The amount of NaOH used in the titration determined the amount of the functional groups in f-MWCNT.

The calculations of the percentage of the functional groups in the f-MWCNT were done by dividing the mole quantity of NaOH obtained from titration by the mole quantity of the f-MWCNT used in titration.

$$\frac{X\ mol\ of\ NaOH}{X\ mol\ of\ f-MWCNT} \times 100$$

The average volume obtained from titration was 12.5 ml of 0.05M NaOH which is equal to 0.63 mmol. The f-MWCNT mole quantity assuming only carbon is present is 4.17 mmol. By putting the values into the equation, the percentage of the functional groups was found to be 15.0%.

The same procedure was done using $NaHCO_3$ instead of NaOH as stirring solution, in order to determine the quantity of carboxylic acid functional groups quantity. The procedure was as follows; 50 mg of f-MWCNT was stirred in 50 ml 0.05 M $NaHCO_3$ for 48 h. under nitrogen atmosphere. The mixture was then filtered and washed with small amount of de-ionized water using 0.20 μm cellulose nitrate filter paper. The combined filtrate and the washings were collected and 50 ml of 0.05 M HCl was added and boiled for 20 min. After cooling to room temperature, the excess HCl was titrated with 0.05 M of NaOH to reach the natural point (pH 7.00), as monitored by a pH meter.

The amount of NaOH used in the titration determined the amount of the functional groups in f-MWCNT.

The average volume obtained from titration was 7.5 ml of 0.05M $NaHCO_3$ which is equal to 0.38 mmol. Dividing this value by the quantity of the f-MWCNT = 4.17 mmol, the percentage of the carboxylic acid functional groups was found to be 8.99%.

3.4 Synthesis of the Catalysts

The synthesis of Pt nanoparticles on the surface of the MWCNTs and f-MWCNT was achieved by impregnation method and hydrogen gas reduction. Pt/MWCNT and Pt/f-MWCNT were synthesized with theoretical amount of 30, 20, and 10 wt%. However, the actual amounts of the Pt wt% were less than the theoretical amounts as was determined by ICP-MS Table 3.1. Figure 3.4 shows the two steps of the formation of the Pt nanoparticles.

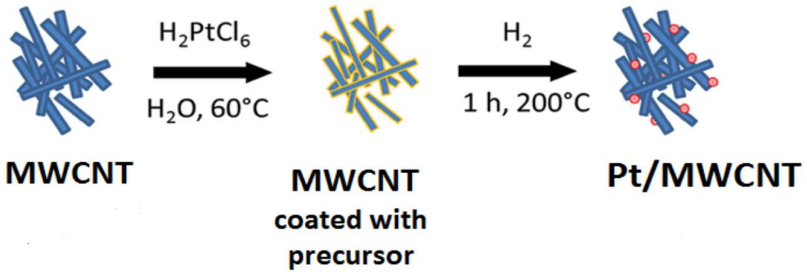

Figure 3.4. Impregnation method steps for Pt nanoparticle synthesis [41]

3.4.1 Synthesis of Pt/MWCNT Nanoparticles

3.4.1.1 Pt/MWCNT 30 wt%

50 mg of MWCNT was dispersed in 8 mL of $9.6x10^{-3}$ M of chloroplatinic acid ($H_2PtCl_6.6H_2O$) solution Table 3.1. The dispersion was sonicated for two hours in sonication bath to achieve good dispersion of the precursor on MWCNT. After that the mixture was dried in the oven at 60 °C for at least 15 hrs. to evaporate all water. The MWCNT deposited with the precursor were collected and put into reduction vessel which was sealed and put into oil bath. Nitrogen gas was flown into the reaction medium with heating until 160 °C was reached. At 160 °C hydrogen gas was allowed into the system and the temperature was kept at 200 °C for 1 h. The vessel was taken out of the oil bath and left to cool at room temperature under nitrogen gas atmosphere. The Pt/MWCNTs nanoparticle catalyst were removed from vessel and were ready for further experimental work.

3.4.1.2 Pt/MWCNT 20 and 10 wt%

Synthesis of the 20 and 10 wt% was done using the same procedure followed for Pt/MWCNT 30 wt% with the appropriate amount of $H_2PtCl_6.6H_2O$. The values used for the Pt precursor (in mg and M), and ICP-MS results are listed in Table 3.1.

3.4.2 Synthesis of Pt/f-MWCNT Nanoparticles

The synthesis of Pt nanoparticles on the surface of the f-MWCNT was done using the same procedure as Pt/MWCNT nanoparticles. 50 mg of f-MWCNT was dispersed in 8 mL of the listed concentration in Table 3.1 of chloroplatinic acid ($H_2PtCl_6.6H_2O$) solution. The dispersion was sonicated for two hours in sonication bath to achieve good dispersion of the precursor on f-MWCNT. After that the mixture was dried in the oven

at 60 °C for at least 15 hrs. to evaporate all water. The f-MWCNT deposited with the precursor were collected and put into reduction vessel which was sealed and put into oil bath. Nitrogen gas was flown into the reaction medium with heating until 160 °C was reached. At 160 °C hydrogen gas was allowed into the system and the temperature was kept at 200 °C for 1 h. The vessel was taken out of the oil bath and left to cool at room temperature under nitrogen gas atmosphere. The Pt/f-MWCNTs nanoparticle catalyst were removed from vessel and were ready for further experimental work.

Table 3.1. Amounts of the precursor used and the actual amount of Pt.

Catalyst	**Amount of MWCNT (mg)**	**Amount of Pt (mg)**	**Amount of precursor (mg)**	**Molarity of the precursor solution (M)**	**Actual amount of Pt (wt%)**
Pt/MWCNT 30 wt%	50	15.0	39.6	9.6×10^{-3}	**17**
Pt/MWCNT 20 wt%	50	10.0	26.3	6.4×10^{-3}	**-**
Pt/MWCNT 10 wt%	50	5.0	13.1	3.2×10^{-3}	**-**
Pt/f-MWCNT 30 wt%	50	15.0	39.6	9.6×10^{-3}	**14**
Pt/f-MWCNT 20 wt%	50	10.0	26.3	6.4×10^{-3}	**10**
Pt/f-MWCNT 10 wt%	50	5.0	13.1	3.2×10^{-3}	**4**

3.5 Preparation of the Electrode Mixtures

The preparation method for the electrode catalyst mixtures was taken from the literature [42]. 10 mg of the prepared catalyst, 0.5 mL of nafion, 0.15 mL of N,N-dimethyl form amide, and 2.0 mL of N-Methyl-2-pyrrolidone were mixed. This mixture was sonicated in ultrasonic bath to obtain a highly dispersed colloidal solution. Then, 40 μL of this slurry solution was dropped on the surface of glassy carbon electrode with 7 mm-diameter and dried at 40 °C for 20 min, 65 °C for 20 min and 100 °C for an hour. This was used as the working electrode.

3.6 Characterization of the Catalysts

The characterization of Pt/MWCNT and Pt/f-MWCNT was done by X-ray Diffraction (XRD), Transmission Electron Microscopy (TEM), X-ray Photoelectron Spectroscopy (XPS), and Inductively Coupled Plasma Mass Spectroscopy (ICP-MS). The activity of the catalysts toward methanol oxidation reaction, and the electrochemical characterization was done using Cyclic Voltammetry (CV) technique.

3.6.1 X-ray Powder Diffraction (XRD)

XRD is an important non-destructive technique for the determination of the crystal structures of metallic elements. XRD working principle is based on the interference of the X-ray beams with one another as they penetrate the crystals of the samples. If an X-ray beam is directed on a crystal, it will be scattered in all directions by the atoms of the crystal. In some directions, an increased intensity is observed due to the constructive interference of the scattered waves. If we direct X-rays with specific angles they are diffracted with different intensities. Measuring the intensity of the diffracted X-ray beams as a function of diffracting angle enables us to determine the crystal structure of the elements [43].

The relationship of the interference of the X-rays with each other and the crystal structure of the elements is explained by Bragg's law:

$$2d\sin\Theta = n\,\lambda$$

Figure 3.5 shows the diffracted X-rays by a crystal based on the Bragg's law. If the incident X-rays of wavelength (λ) is directed to a crystal with specific angle (Θ) where all atoms are placed periodically with planar spacing (d), diffraction beam of sufficient intensity is detected only when the Bragg's law is satisfied [43].

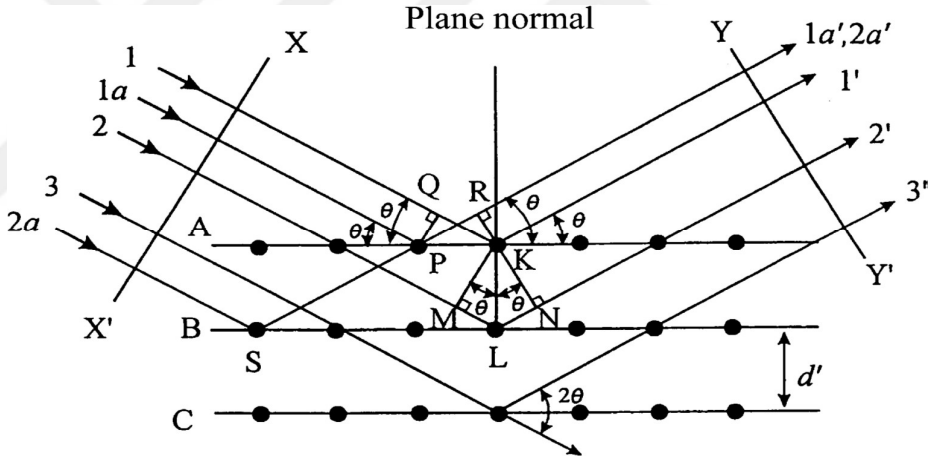

Figure 3.5. Bragg's law diffraction [43]

The possible planer spacing (d) is defined by the indices (h, k, l) which are determined by the shape of the unit cell. Then we can rewriting Bragg's law as follows:

$$\sin\Theta = \lambda/2d$$

Therefore the possible angle values where we can have reflections are determined by the unit cell dimensions. This enables us to determine the crystal structure of the elements by the measurement of the intensity of the X-rays diffracted changing the angle of the directed X-rays. This is achieved using a diffractometer. Figure 3.6 shows the structure and the working principle of the XRD diffractometer.

XRD measurements were carried out by using Rigaku Miniflex diffractometer with Ultima + theta-theta high resolution goniometer and X-ray source (Cu Kα radiation, λ= 1.54056 Å) in chemistry department at METU.

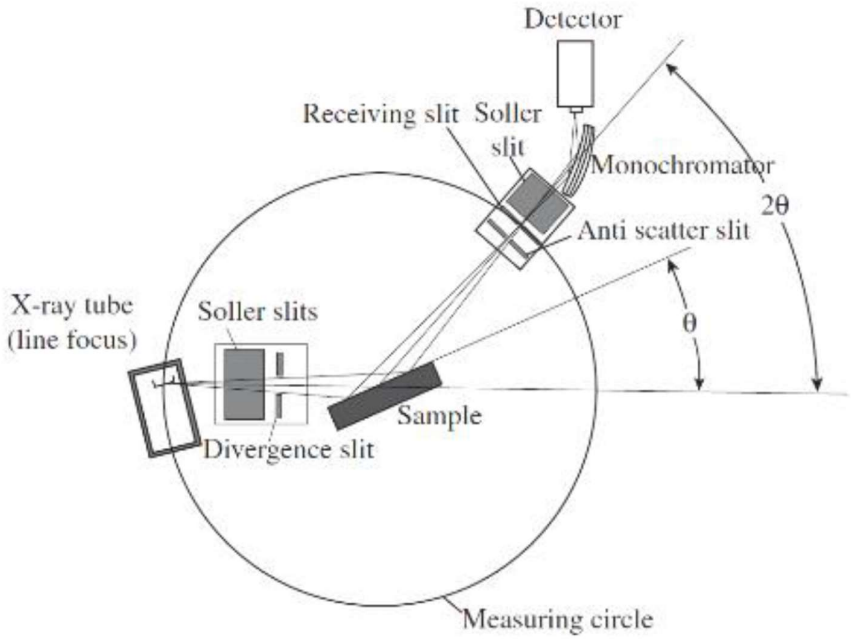

Figure 3.6. Structure and working principles of XRD instrument [44]

3.6.2 Transmission Electron Microscopy (TEM)

Electron microscopy can be defined as the field of science that employs the electron microscope as a tool and uses a beam of electrons to form an image of a sample. The electron microscope takes advantage of the very short wavelength of the electron which is around $\lambda = 0.005$ nm. Electrons interact with atomic particles of the samples which enables us to draw images of the samples. The samples can be magnified 500 to 500,000 times their original size which gives us the ability to study the materials in the nanometer size [45].

When an accelerated beam of electrons is directed to a sample, a rich variety of interactions take place. One of the interactions that occurs during the collision of the electron beam and the sample is the direct transmission of electrons. TEM technique projects electrons through an ultrathin slice of the sample and produces a two dimensional image [45]. The TEM instrument can be divided into three parts: the electron source, the objective lens, and the imaging system. The electrons are produced by electron gun with an energy in the range 20 - 1000 keV. Then they are sent to the specimen with a desired diameter using electromagnetic lens. The imaging system uses several lenses to magnify the image and focuses them on the computer display via a detector. Figure 3.7 shows the structure of TEM instrument [46].

In this study the catalysts samples were prepared for TEM analysis by the dispersion of small amount of the Pt/MWCNT powder sample in carbon tetrachloride and small amount of Pt/f-MWCNT powder in ethanol. The mixture was sonicated for short period of time until good dispersion was obtained. Then few drops were dropped upon cupper grid and left to dry in atmosphere. The slit was then introduced to the instrument. TEM images of the samples were taken by JEOL 200 kV TEM instrument in Central Laboratory at METU.

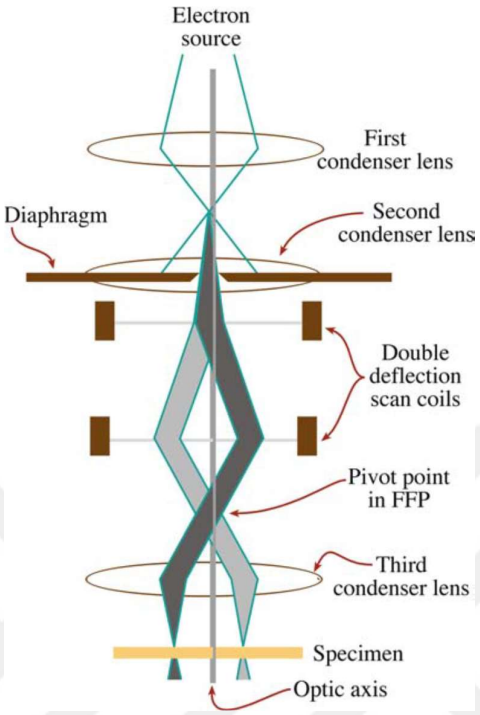

Figure 3.7. TEM instrument [46]

3.6.3 X-ray Photoelectron Spectroscopy (XPS)

XPS analysis reveals the oxidation states of the formed Pt nanoparticles. This could be achieved by fitting the Pt 4f peaks with the cross bonding theoretical peaks. The working principles of XPS analysis is mentioned in section 3.3.2 on page 33. The analysis of Pt samples was done with the same instrument in METU Central Laboratory.

3.6.4 Inductively Coupled Plasma Mass Spectrometry (ICP-MS)

ICP-MS enables quantitation at the parts per million (ppm) levels. Pt nanoparticles are synthesized in very small quantities which makes ICP-MS suitable technique for mass determination. The working principle of ICP-MS is based on the detection of the amount of the elements by the detection of their deflected ions. The elements are ionized first and then sent into mass separation device (mass spectrometer) [47]. Mass spectrometer separates the ions according to their mass to charge ratios. Figure 3.8 shows the basic components of ICP-MS system.

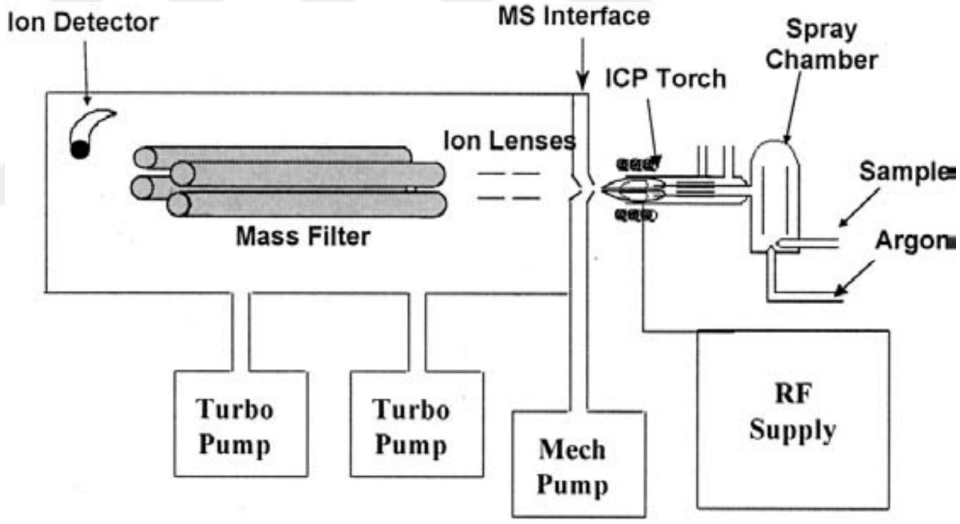

Figure 3.8. ICP-MS instrument [47]

The instrument consist of ionization system, ion focusing system, mass separation device, and detector. The sample in a liquid form is converted to positively charged ions by the plasma torch. Once the ions are produced in the plasma, they are directed into the mass spectrometer via the interface region. Then the ions using ion lenses are focused into the mass separation device. Mass separation device allows the ions of a

particular mass-to-charge ratio through to the detector and filter out all the interfering, and matrix ions. The final process is to convert the ions into an electrical signal with an ion detector [47].

The ICP-MS analysis was performed with Leeman Lab inductively coupled plasma spectroscopy. The measurements were performed at METU Central Laboratory.

3.6.5 Cyclic Voltammetry (CV)

Cyclic voltammetry (CV) is an important analytical technique for the studies of oxidation and reduction processes and for the determination of adsorption processes on surfaces. It is based on changing the applied potential at a working electrode in both forward and reverse directions while monitoring the current [48].

In CV a continuously time varying potential is applied at constant rate to the working electrode. This results in the occurrence of oxidation or reduction reactions of electroactive species in solution, possibly adsorption of species according to the potential, and a capacitive current due to double layer charging. The potential scan is done with two directions, as shown in figure 3.9 (a) it starts at V1 then is reversed when reaching V2 and swept back to V1 [49]. This gave us a cycle which is shown in figure 3.9 (b).

CV was carried out in an electrochemical cell containing electrolyte with three electrode arrangement. The three electrodes are; working electrode, reference electrode, and counter electrode. In our measurement we used glassy carbon with diameter of 7mm as the working electrode. The reference electrode was Ag/AgCl electrode and the counter electrode was platinum wire.

Measurements were carried out in 0.1 M $HClO_4$ and 0.1 M $HClO_4$ + 0.5 M CH_3OH electrolyte solutions for each catalyst at room temperature using computer-controlled potentiostat / galvanostat (Solartron 1285) in Chemistry Department of METU.

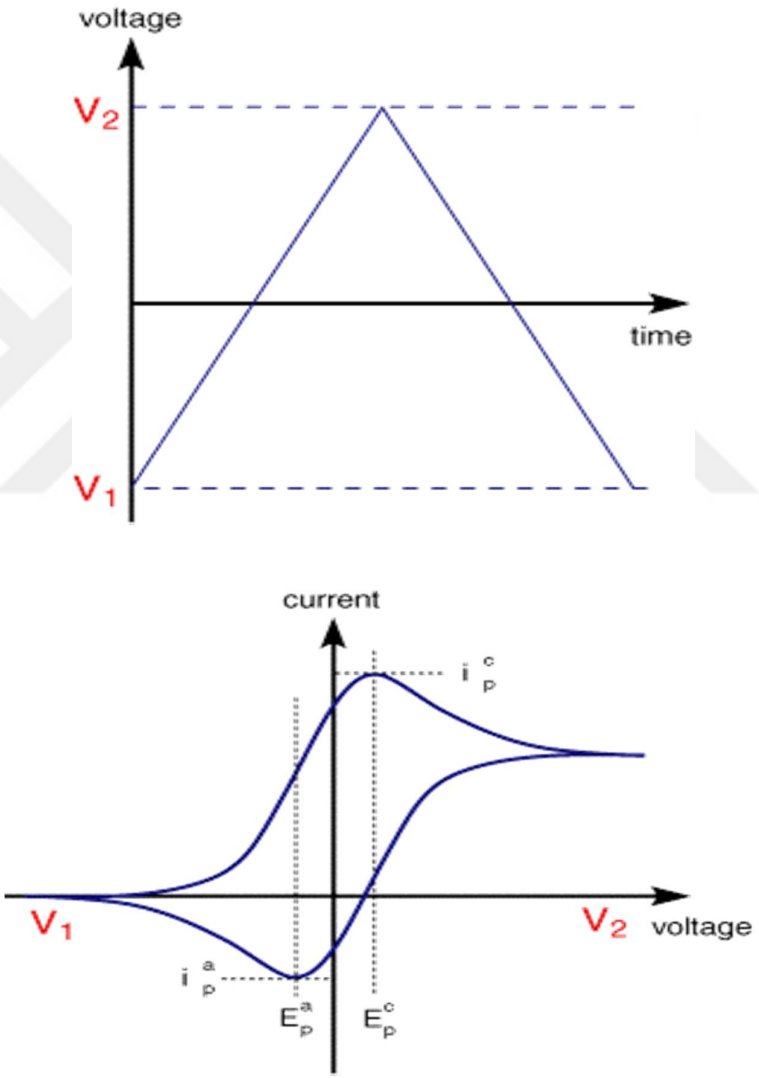

Figure 3.9. a) Voltage versus Time graph, b) Current versus Voltage graph [48]

CHAPTER 4

RESULTS AND DISCUSSION

4.1 Characterization of the f-MWCNT

The sonochemical treatment of the MWCNTs in acidic solution results in the oxidation of the sp^2 carbon atoms and formation of oxygen containing groups (carboxylic, carbonyl, and hydroxyl) [26, 27, 35, 49, 50] as shown in Figure 4.1. The formation of these groups in the f-MWCNT was analyzed by FTIR, XPS and acid-base titration.

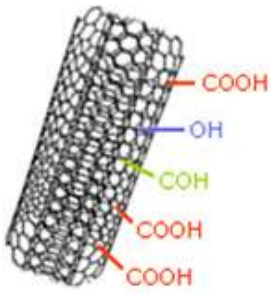

Figure 4.1. Representation of the functional groups attached to the CNT [36]

4.1.1 Fourier Transform Infra-Red Spectroscopy (FTIR)

The FTIR spectra were obtained in the middle infrared region (400 - 4000 cm^{-1}). The type of the functional group can be generally determined by the region in which it is located in the spectrum, though there might be some shifts in the measured position of

the vibrational bands [52]. The vibrations that are found in the middle infrared region for the f-MWCNT are related to O-H, C-H, C-O, and C=O [52, 53]. In general, the fundamental vibrations in the 4000 - 2500 cm^{-1} region are generally due to O–H and C–H stretching. O–H stretching produces a broad band that occurs in the range 2700 - 3600 cm^{-1}. C–H stretching bands occur in the range 3000 - 2850 cm^{-1}. The principal bands in the 2000–1500 cm^{-1} region are due to C=C and C=O stretching. Carbonyl stretching depending on the type of C=O bond, occurs in the 1830 - 1650 cm^{-1} region [52]. The band in the 1500 - 650 cm^{-1} region has many vibrations which are not so well behaved and may vary by hundreds of wavenumbers [55]. Table 4.1 shows the expected functional groups and their corresponding peak position (cm^{-1}) in the IR spectrum.

Table 4.1. Expected functional groups and their IR band in wavenumbers [52, 54]

Wavenumber (cm^{-1})	**Assignment**
Aromatic structure of CNT:	
3100–3000	C–H stretching
1600–1430	C=C stretching
1275–1000	In-plane C–H bending
900–690	Out-of-plane C–H bending
Oxygen containing groups:	
Hydroxyl	
3550–3500	Phenol O–H stretching
1300–1000	C–O stretching
Carbonyl	
1600–1700	C=O stretching

Carboxylic acids	
3300–2500	O–H stretching
1700–1730	C=O stretching
1430	C–O–H in-plane bending
1240	C–O stretching
930	C–O–H out-of-plane bending

The FTIR spectrum of the f-MWCNTs and MWCNTs are shown in the Figure 4.2. As can be seen from the figure, the FTIR spectra for MWCNT and f-MWCNT are extremely different from each other. There is almost no peaks found in the MWCNT spectrum. In the other hand, the f-MWCNT spectrum shows various peaks with different intensities and shapes. These peaks are assigned to the oxygen based functional groups which have C-O, C=O, and O-H vibration bands and to the structure of MWCNT which shows C-H and C=C vibration.

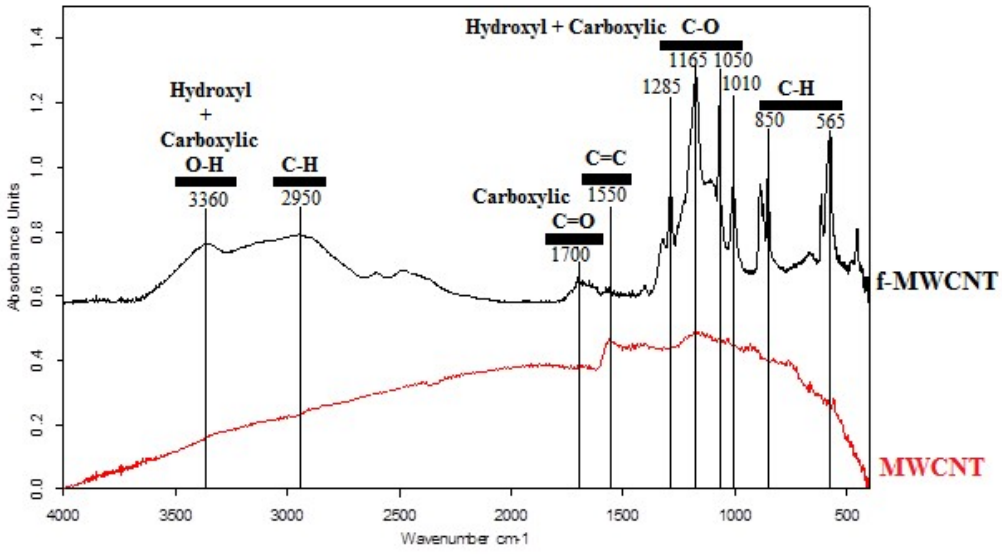

Figure 4.2. FTIR spectrum for MWCNT and f-MWCNT

The broad peaks at 3360 and 2950 cm^{-1} were assigned to the hydroxyl plus carboxylic O-H stretching and to C-H stretching, respectively. Carboxylic C=O stretching was observed at 1700 cm^{-1} and C=C stretching which is the backbone of the MWCNT was observed at 1550 cm^{-1}. The intense peaks between 1010 and 1285 cm^{-1} were due to the C-O stretching of the hydroxyl and the carboxylic groups. The other two sharp peaks at 565 and 850 cm^{-1} were assigned to the out-of-plane and in-plane C–H bending [53]. The strong and the sharp peaks that were assigned to C-O stretching between 1010-1285 cm^{-1} may also belong to SO_2 asymmetric stretching, SO_2 symmetric stretching, and S=O stretching from the sulfate groups remaining on the f-MWCNT after the functionalization procedure in which sulfuric acid was used. To determine which type of the groups belong to this region XPS analysis was performed for the f-MWCNT samples. The results showed very few amount of sulfur (0.15%) therefore, these peaks are assigned for C-O groups.

4.1.2 X-ray Photoelectron Spectroscopy

In general, XPS is a powerful technique for the study of the composition and the chemical states of varies elements. Here, it is used to determine the composition and the relative quantities of the functional groups that were formed after functionalization.

XPS spectra for MWCNT and f-MWCNT are shown in Figure 4.3. The spectrum of the MWCNT consists of 99.43% carbon and 0.57% oxygen at 284 and 530 eV respectively [56]. The f-MWCNT spectrum consists of 86.73% carbon, 13.13% oxygen, and 0.15% sulfur. These values were obtained from the relative peak areas of the C 1s, O 1s, and S 2p at 284, 530, and 168 eV respectively [57]. Obviously, these results illustrate the increased amount of oxygen in the f-MWCNT due to the functionalization and the remaining of small amount of sulfur from the sulfuric acid used in the process.

The XPS analysis was used to determine the types of the functional groups and their relative quantities. For this purpose, the C 1s, O 1s and S 2p regions of the spectrum of the MWCNT and f-MWCNT were analyzed. Gaussian-Lorentzian method was used for fitting XPS peaks and the background was subtracted by means of Shirley's method. All peaks were analyzed in terms of relative peak area and chemical shifts of C, O and S. The C 1s peak at 284.6 eV was taken as the reference and charging effects were corrected according to this value.

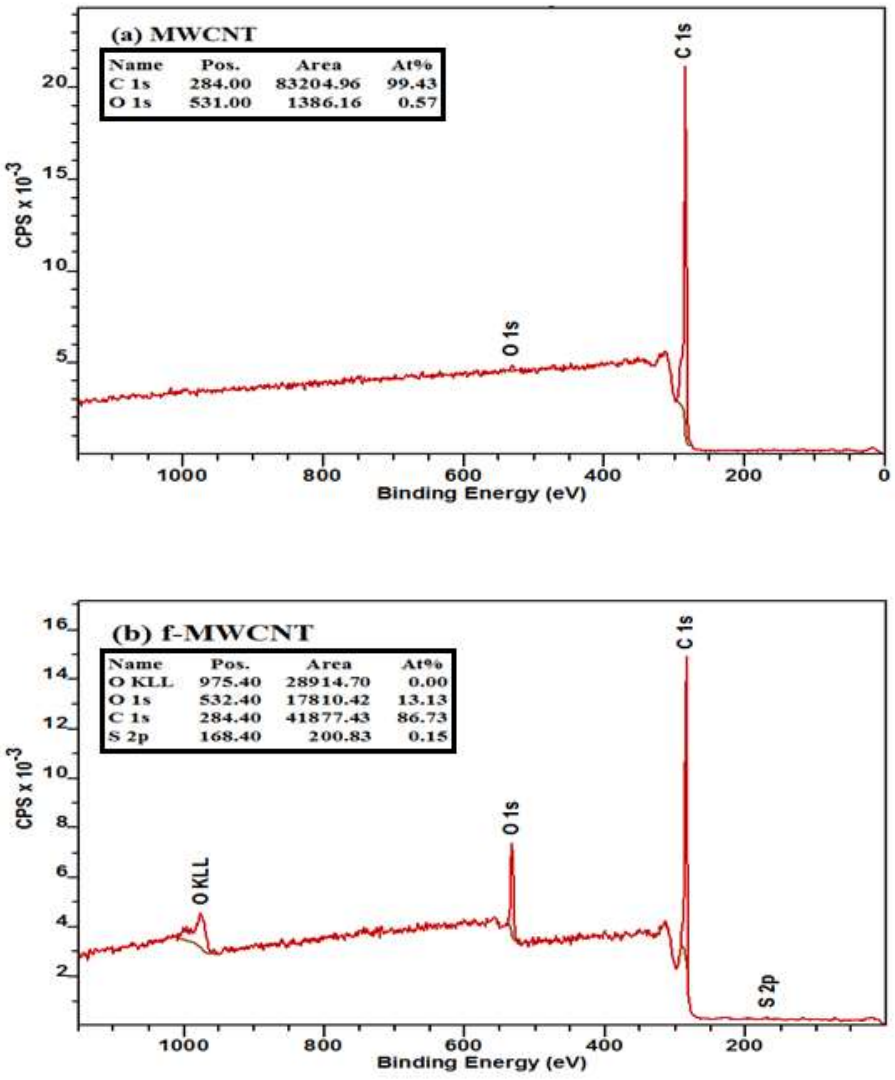

Figure 4.3. XPS spectrums for (a) MWCNT and (b) f-MWCNT

Figure 4.4 shows the analyzed C 1s peak for MWCNT and f-MWCNT. There are two peaks found in MWCNT peak which are assigned to C sp^2 at 284.62 eV and π-π* transition at 290.52 eV [56] with no appearance of carbon oxygen peaks. In the case of f-MWCNT, six peaks are found which are assigned to C sp^2, C sp^3, C-O, C=O, O-C=O, and π-π* transition with the binding energy values of 284.58, 285.43, 286.20, 287.02, 288.73, and 290.59 eV, respectively [57]. The percent quantities of each functional group is found from the percent relative area of its correspondent peak. The highest quantity is found to be for carboxylic O-C=O group with 8.52% followed by hydroxyl C-O group with 7.02% and carbonyl C=O group with 4.37%.

The analyzed O 1s and S 2p peaks for f-MWCNT are shown in Figure 4.5. O 1s peak at 532 eV contains five peaks which are assigned for C=O, C-O, O-C=O, SO_4 and H_2O with binding energy values of 532.14, 533.21, 534.39, 532.72 and 538.04 eV respectively [53, 58, 59]. The small peak at 538.04 eV is resulted from the occluded H_2O molecules on the surface of the f-MWCNT [35]. The highest relative percent area found to be for O-C=O with 50.39% followed by C-O with 27.23% and C=O with 16.00%. The SO_4 and H_2O have small relative areas with 0.15% and 5.64%, respectively. The S 2p peak at 168 eV shows doublet shape peak for $2p_{3/2}$ and $2p_{1/2}$ as shown in Figure 4.5 (b). These peaks are assigned for sulfate groups which remained from sulfuric acid used in functionalization. The small area of this peak (0.15%) indicates the small quantity of the sulfate groups in the f-MWCNTs.

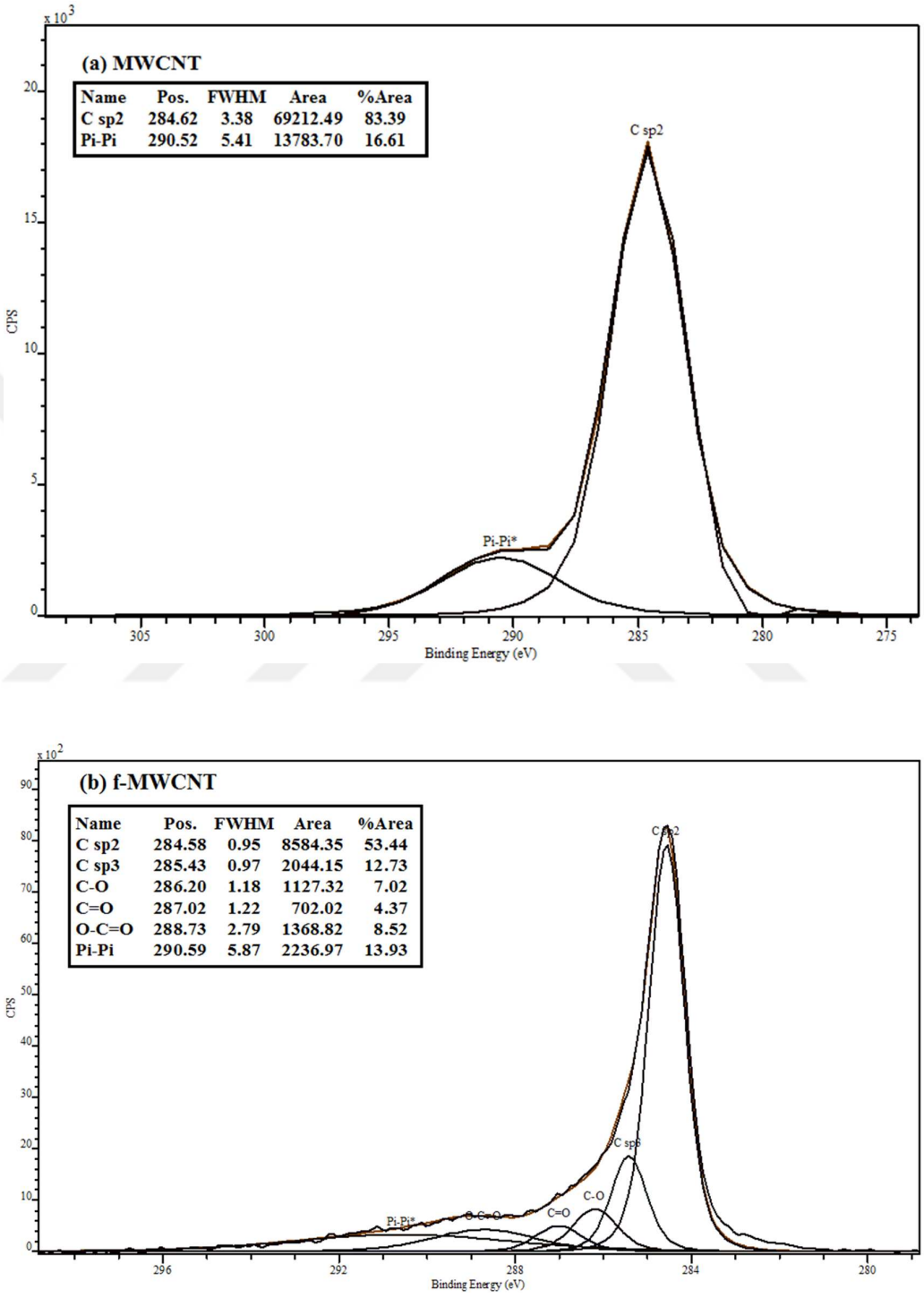

Figure 4.4. XPS peak fitting for C1s peak for (a) MWCNT and (b) f-MWCNT

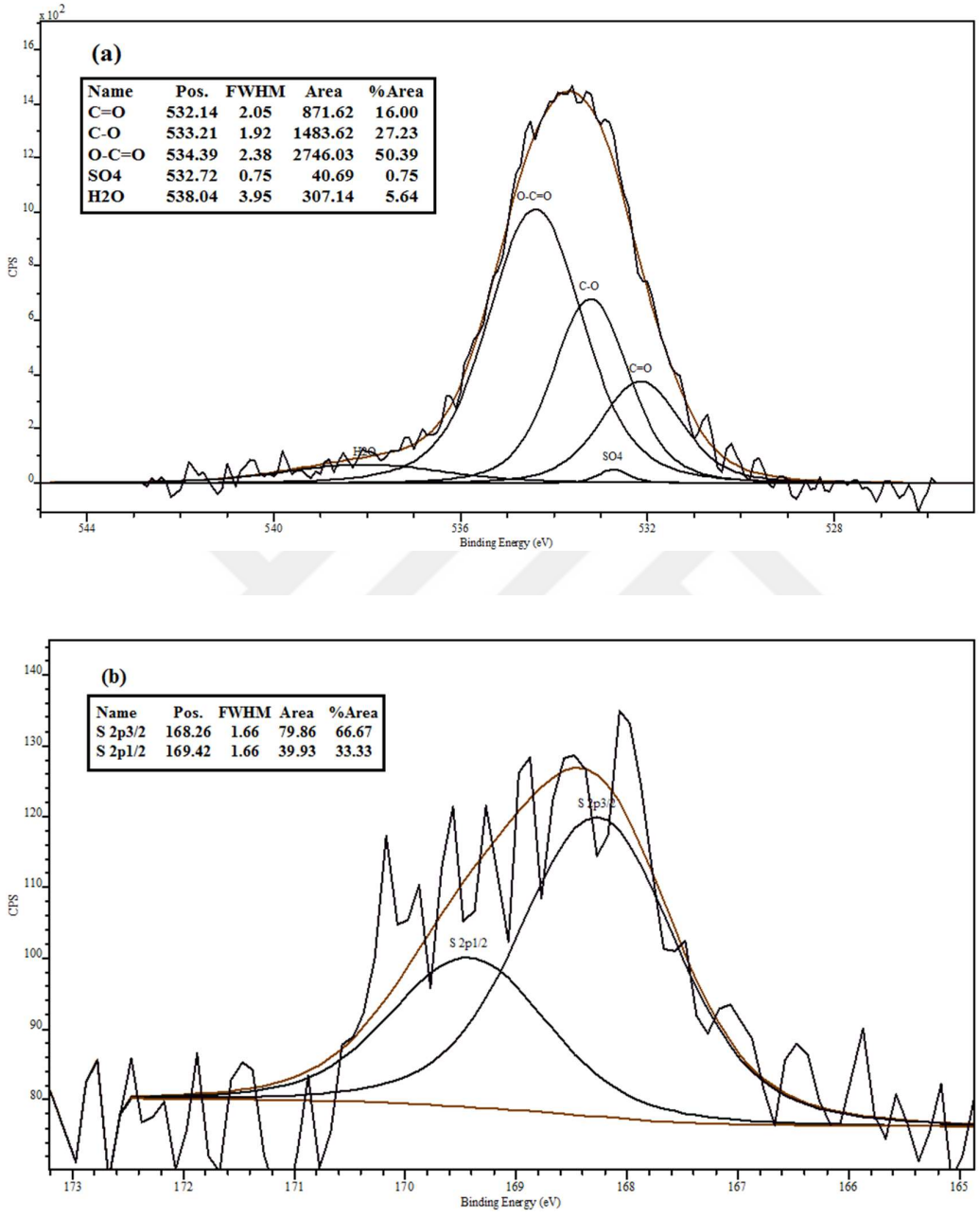

Figure 4.5. XPS fitting peaks for (a) Oxygen 1s and (b) Sulfur 2p for f-MWCNT

4.1.3 Acid-Base Back Titration for f-MWCNT

From the titration of the functional-MWCNT with NaOH the quantity of acidic sites in f-MWCNT were calculated. The mole quantities of NaOH used in the titration were the same as mole quantities of acidic sites (oxygen containing groups). This is because Na^+ ions were exchanged with H^+ ions of the oxygen functional groups. The titration procedure can be shown by the following reactions:

$$\mathrm{MWCNT-COOH\ or\ COH + NaOH(excess)} \rightarrow \mathrm{MWCNT-COO-Na^+\ or\ CO{-}Na^+ + NaOH(determined\ by\ titration)}$$

It can be seen from the reaction equation that the only oxygen containing groups that are determined by the titration are the protic functional groups (carboxyl and hydroxyl) [60]. The value obtained can be assigned to the carboxylic and the hydroxyl groups in the f-MWCNT.

The average value of weight percent of acidic sites was around 15.2% and 8.9% for carboxylic acid sites. This result shows the high quantity of oxygen containing groups resulted from our sonochemical treatment of the MWCNT and in close agreement with the XPS results.

4.2 Characterization of Pt/MWCNT and Pt/f-MWCNT Catalysts

4.2.1 Inductively Coupled Plasma Mass Spectrometry (ICP-MS)

The quantities of Pt in each catalyst were measured using ICP-MS technique. Table 4.2 shows the percentage of Pt in each sample plus the amount in milligram of Pt used in the electrodes for electrochemical measurement (CV). It is noticed that the amount of the Pt in each sample is almost half the theoretical amounts. This decrease in the amount of Pt is caused by the preparation procedure. In our procedure we dried the

mixture of precursor and support to evaporate all water molecules and to obtain solid powder. We believe some amount of the precursor was lost during this process. It is also possible that some of the precursor was lost during the reduction process where 200 °C was applied to the samples.

The ICP-MS measurements were not performed for the Pt/MWCNT 20 and 10 wt% due to their poor activity in the methanol oxidation reaction.

Table. 4.2. Quantities of Pt% in each catalyst and the used electrodes

Catalyst with theoretical Pt quantity	**Pt (%)**	**Pt amount in one electrode (mg)**	**Catalyst with actual Pt quantity**
Pt/MWCNT 30%	17.0	0.03293	Pt/MWCNT 17%
Pt/f-MWCNT 30%	14.1	0.02731	Pt/f-MWCNT 14%
Pt/f-MWCNT 20%	10.1	0.01956	Pt/f-MWCNT 10%
Pt/f-MWCNT 10%	3.76	0.00728	Pt/f-MWCNT 4%

4.2.2 X-ray Diffraction (XRD)

X-ray powder diffraction patterns of all prepared catalysts indicated that Pt has a faced center cubic structure. Figure 4.6 (a) shows the XRD patterns of Pt/MWCNT (theor.10, theor.20, 17 wt%). The first peak is assigned for C (002) at 2θ = 26.2 which is graphite peak from MWCNT structure. The other peaks are assigned to Pt (111), Pt (200), Pt (220), and Pt (311) with 2θ = 39.9, 46.3, 67.5, and 81.2, respectively. These peaks are broad which is characteristic of nanoparticles [43].

The XRD patterns for Pt/f-MWCNT (14, 10, 4 wt%) samples are shown in Figure 4.6 (b). The patterns show the same results with the Pt/MWCNT peaks at about $2\theta = 25.4$, 39.9, 46.4, 67.7, and 81.6 which are assigned for C (002), Pt (111), Pt (200), Pt (220), and Pt (311), respectively.

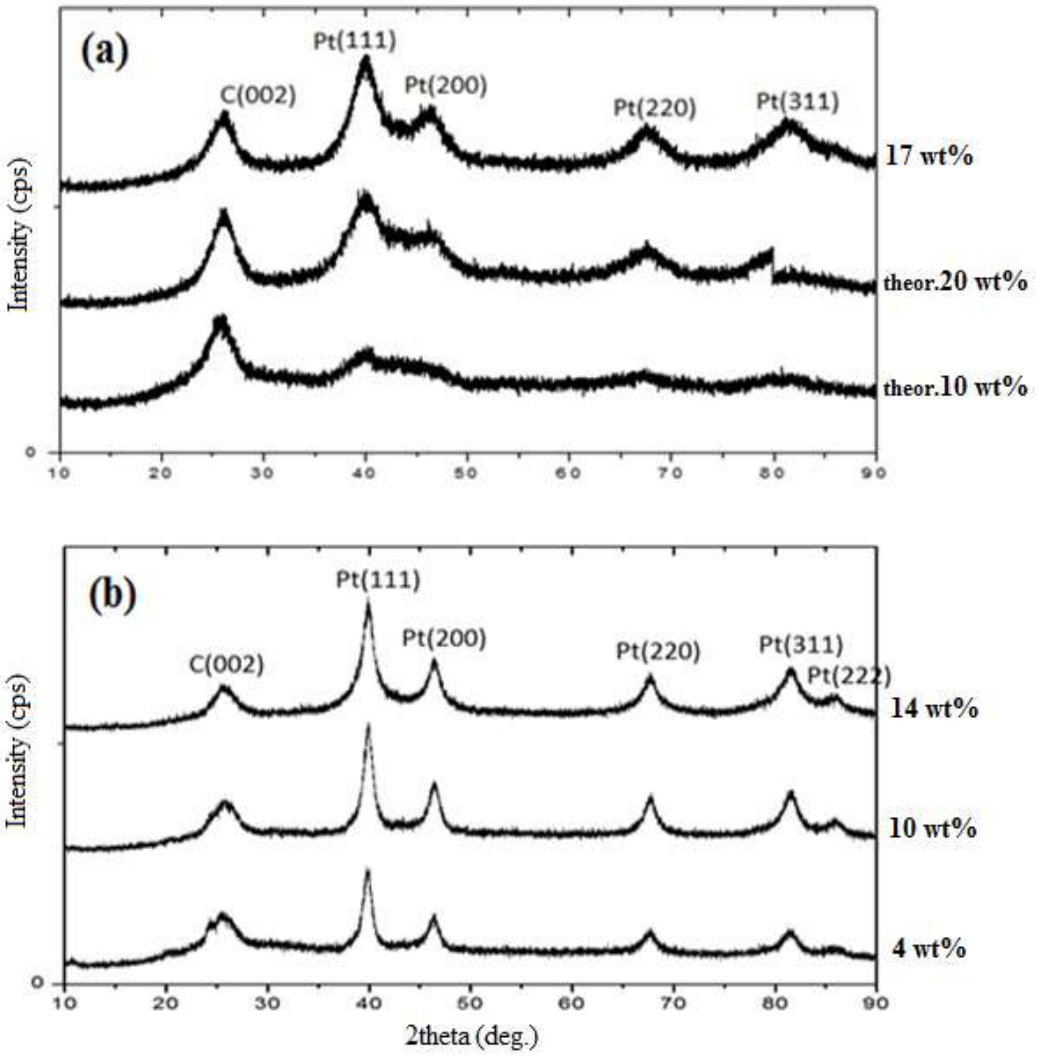

Figure 4.6. XRD patterns for (a) Pt/MWCNT (17, theor.20 and theor.10 wt%), (b) Pt/f-MWCNT (17, 10 and 4 wt%)

The particle size of the Pt nanoparticles can be estimated based on the full width half maximum of the Pt peaks using the Scherrer equation [43];

$$d\,(\text{Å}) = \frac{k\lambda}{\beta\, cos\theta}$$

Where,

k = coefficient (0.9)

λ = the X-ray wavelength (1.54056 Å)

β = the full width half-maximum of the Pt (200) diffraction peak (rad)

θ = the angle at the position of peak maximum (rad)

Table 4.2 shows the estimated values for the particle sizes for each sample based on calculations of Scherrer equation. The values for the Pt/MWCNT with nominal values 10 and 20 wt% show very small particle sizes of 0.5 and 1.1 nm and larger particle size of 1.6 for Pt/MWCNT 17 wt%. The values for Pt/f-MWCNT showed larger particles with 2.1, 3.6 and 3.8 for 4, 10 and 14 wt% respectively.

The increase in size with the amount of Pt is related to the formation mechanism of the Pt nanoparticles on the surface of the MWCNT. The bottom-up approach for the formation of the nanoparticles is a two steps process. These steps are nucleation and growth [61] [62]. The nucleation and the growth of the supported Pt nanoparticles occur on the surface of the MWCNT with the reduction of the precursor. The adsorption of higher quantities of the precursor on the surface of the MWCNT, which is the result of higher quantity of the precursor added, leads to larger growth of the formed Pt nanoparticles.

The increase in the particle sizes between the Pt/f-MWCNT to Pt/MWCNT is related to the modification of the surface of MWCNT by functionalization. The introduction of the oxygen functional groups to the MWCNT increased the dispersion of the precursor on f-MWCNT. This is due to the increase in the electrostatic adsorption of

the anionic precursor on the surface of the MWCNT [30, 31, 61]. The increase of the adsorption lead to larger growth of the Pt nanoparticles as mentioned above.

Table 4.3. Average particle sizes for Pt nanoparticles from XRD

Catalyst	Average particle size(nm)
Pt/MWCNT 17 wt%	1.6
Pt/MWCNT theor.20 wt%	1.1
Pt/MWCNT theor.10 wt%	0.5
Pt/f-MWCNT 14 wt%	3.8
Pt/f-MWCNT 10 wt%	3.6
Pt/f-MWCNT 4 wt%	2.1

Due to the very poor activity as a catalyst in the methanol oxidation reaction, further characterizations of Pt/MWCNT theor.10 and theor.20 wt% were not performed as stressed before.

4.2.3 Transmission Electron Microscopy (TEM)

To solidify the result obtained from XRD data and to investigate the individual size, shape, and Pt nanoparticle distribution on the support, the catalysts were examined by TEM technique. Figure 4.7 contains the TEM images of 17 wt% for Pt/MWCNT and 14 wt% for Pt/f-MWCNT. The difference in the shapes of Pt nanoparticles in Pt/MWCNT and Pt/f-MWCNT can be seen clearly from the TEM images. Pt

nanoparticles formed on the surface of the f-MWCNT are spherical and evenly distributed over the surface Figure 4.7 (b). In the other hand, different shapes including spherical nanoparticles, linear shaped particles, and agglomerated particles are seen for the Pt nanoparticles formed on MWCNT Figure 4.7 (a). This result confirms the positive effect of the functional groups on the formation of narrow distributed Pt nanoparticles on the surface of f-MWCNT.

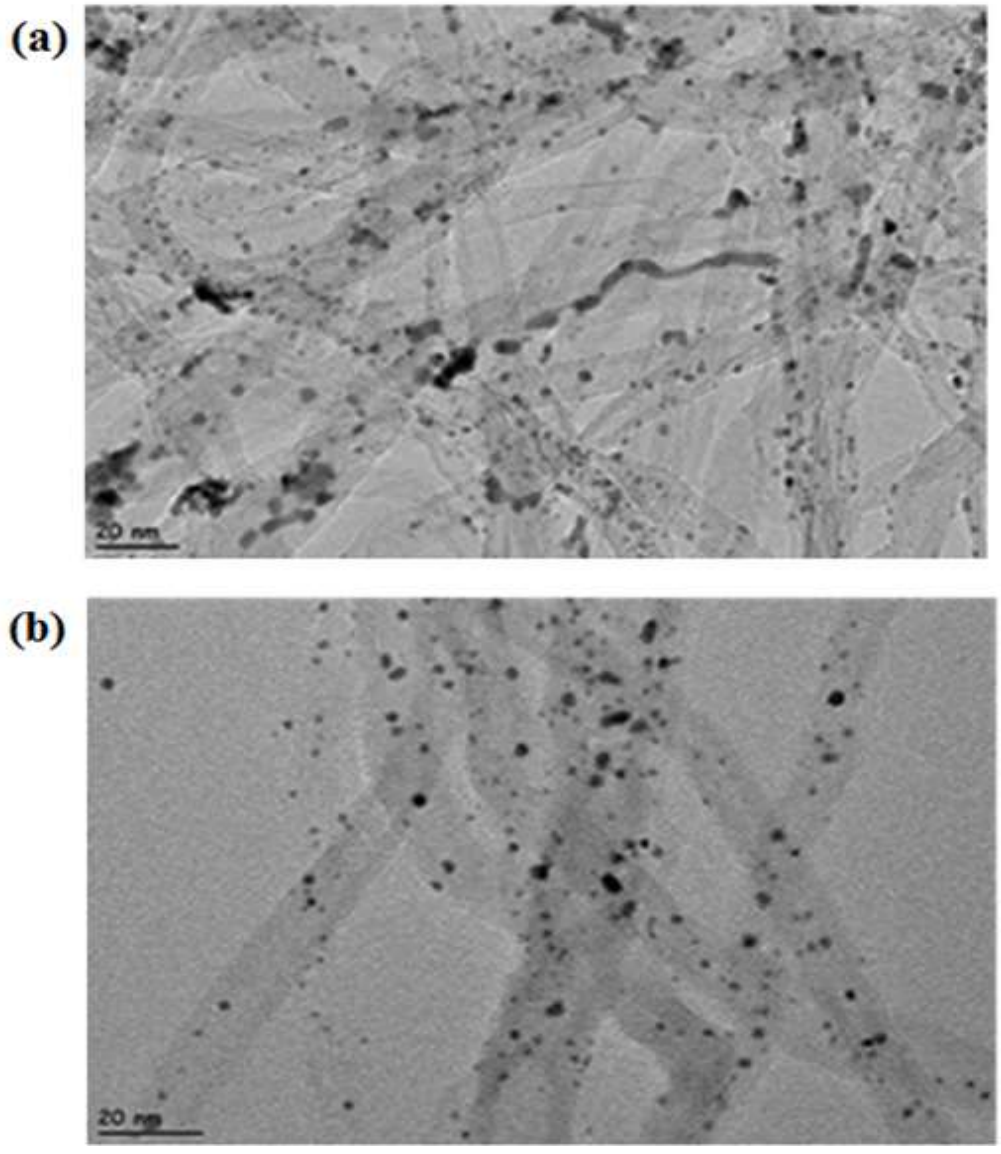

Figure 4.7. TEM images of (a) Pt/CNT 17 wt%, (b) Pt/f-CNT 14 wt%

As stated in XRD, the higher adsorption of the precursor on the f-MWCNT results in the larger average particle size and the functional groups increase the adsorption of the precursor. Moreover, functional groups have major effect on particle distribution by aiding the precursor to be evenly distributed over the surface of the f-MWCNT [31, 61]. This effect can be seen from the TEM images of Pt/MWCNT 17 wt% and Pt/f-MWCNT 14 wt% samples in Figure 4.7. In the case of Pt/f-MWCNT 10 and 4 wt% samples, spherical nanoparticles were formed with good size distribution as can be seen from figure 4.8 (a) and (b).

The average particle sizes of the Pt nanoparticles were calculated using Fiji computer program [64] with the counting of at least 250 particles in each sample. The calculation of the average particle sizes was done without the agglomerated particles consideration. The values of the average particle sizes are shown in the Table 4.3. By comparing the XRD size values with the values calculated from TEM images, we notice similar values with no big changes. The histograms are also shown in Figure 4.4. In general, TEM and XRD results indicated the same trend in the size of Pt nanoparticles.

Table 4.4. Average particle sizes obtained from TEM and XRD

Catalyst	**TEM Particle size (nm)**	**XRD Particle size (nm)**
Pt/MWCNT 17 wt%	1.95 ± 0.32	1.6
Pt/f-MWCNT 14 wt%	2.74 ± 0.58	3.8
Pt/f-MWCNT 10 wt%	2.70 ± 0.56	3.6
Pt/f-MWCNT 4 wt%	2.57 ± 0.62	2.1

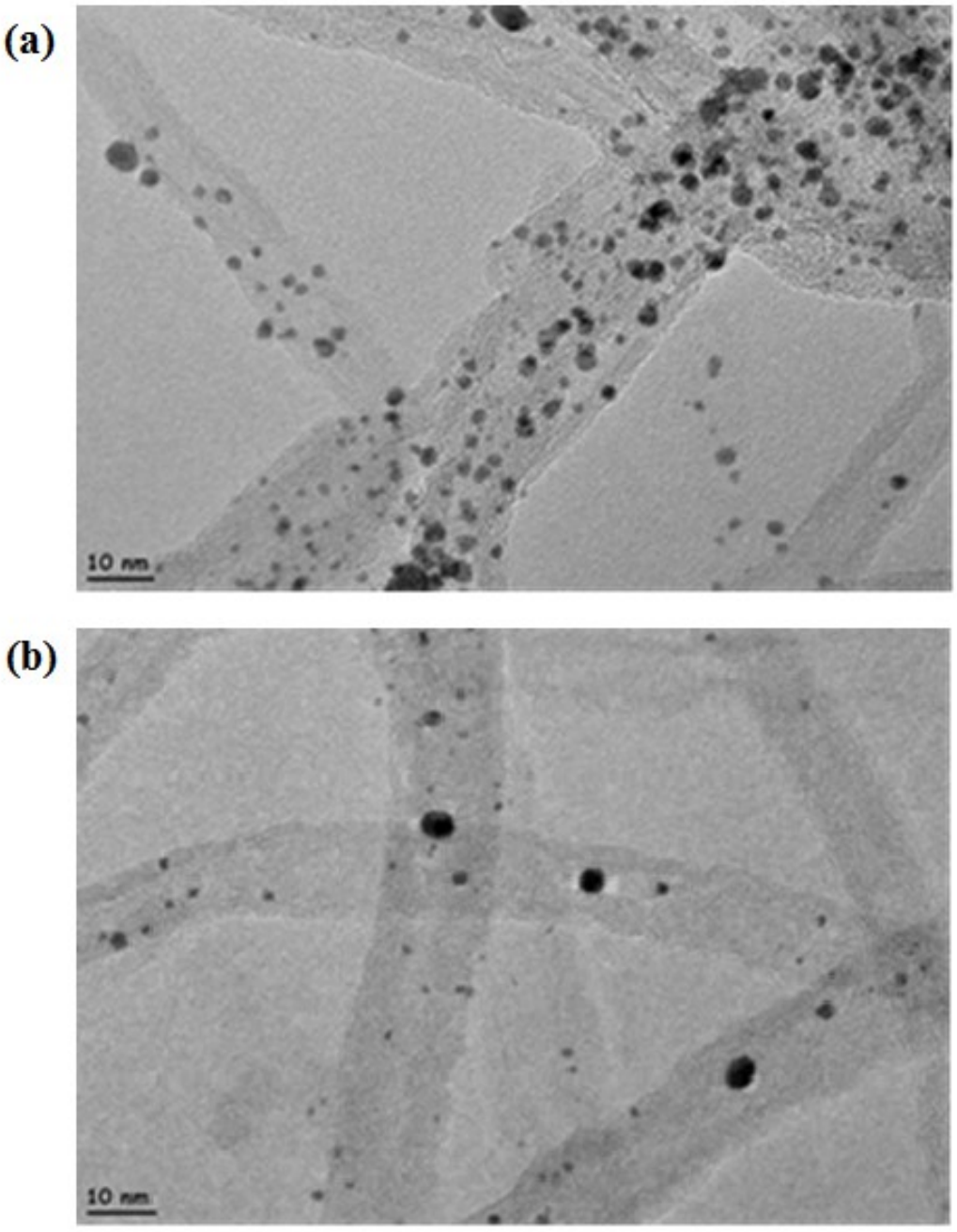

Figure 4.8. TEM images of (a) Pt/f-MWCNT 10 wt%, (b) Pt/f-MWCNT

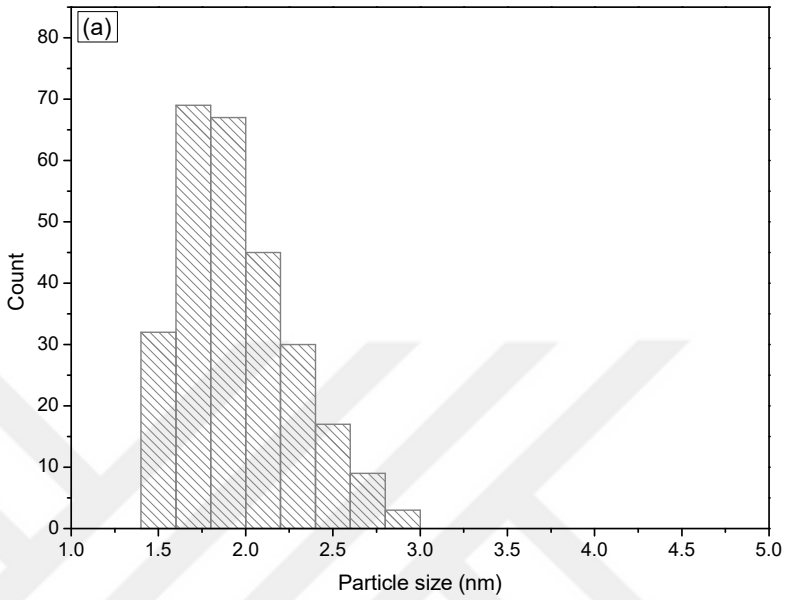
(a)
Count
Particle size (nm)
0
10
20
30
40
50
60
70
80
1.0
1.5
2.0
2.5
3.0
3.5
4.0
4.5
5.0

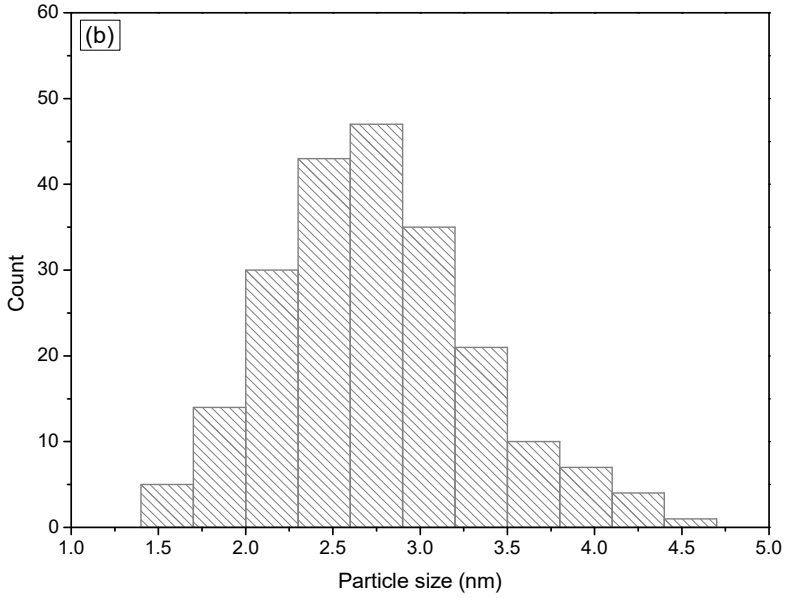
(b)
Count
Particle size (nm)
0
10
20
30
40
50
60
1.0
1.5
2.0
2.5
3.0
3.5
4.0
4.5
5.0

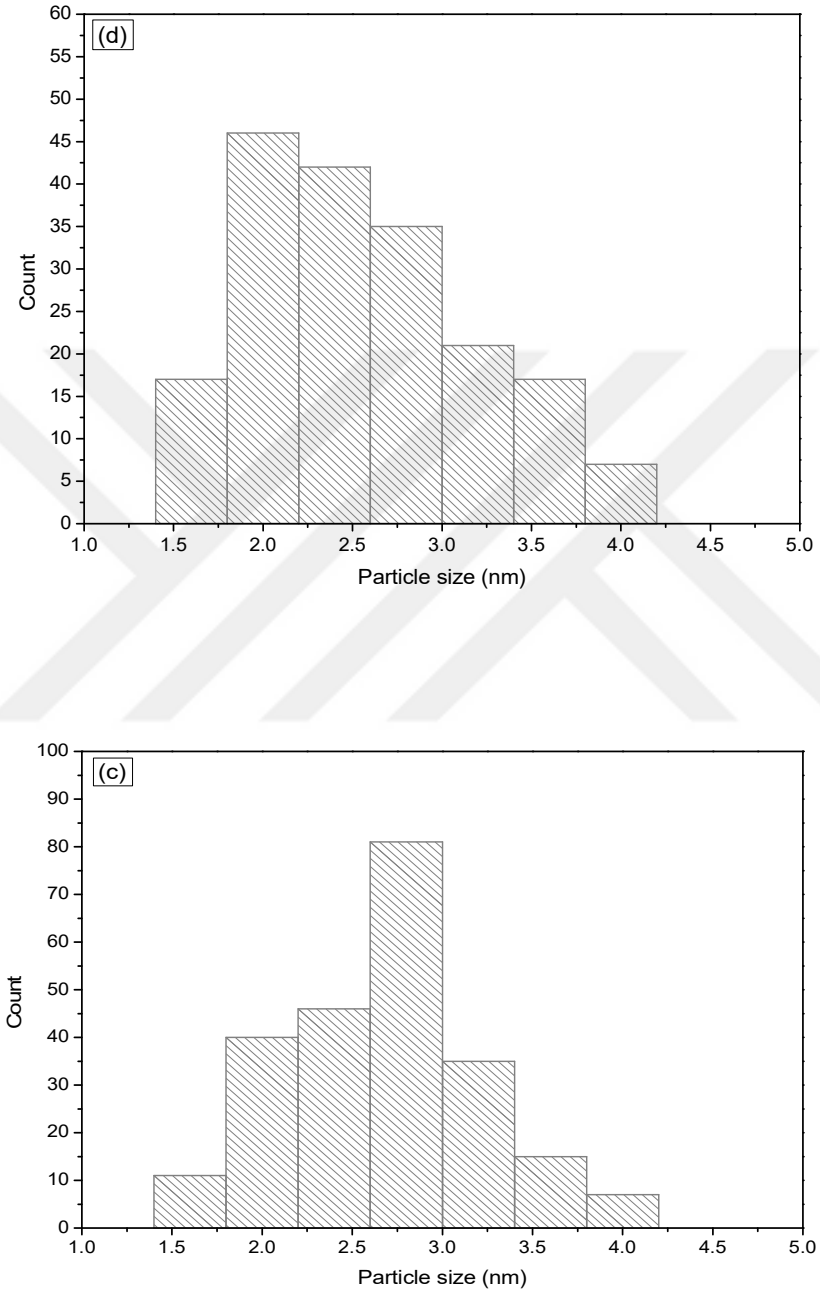

Figure 4.9. Size distribution histograms measured by TEM for (a) Pt/MWCNT 17 wt%, (b) Pt/f-MWCNT 14 wt%, (c) Pt/f-MWCNT 10 wt%, (d) Pt/f-MWCNT 4 wt%

4.2.4 X-ray Photoelectron Spectroscopy (XPS)

The oxidation states of the platinum nanoparticles were investigated using XPS technique. The full spectra that were obtained for (Pt/CNT 17 wt% and Pt/f-CNT 14 wt%) are shown in Figure 4.5. The Pt 4f, C 1s, and O 1s are theoretically known to be at 71.1, 284.6, and 532.2 eV respectively which appear in the obtained spectra. The investigation of the Pt 4f peak reveals the oxidation states of the Pt nanoparticles. Gaussian-Lorentzian method was used for fitting XPS peaks and the background was subtracted by means of Shirley's method. C 1s peak was taken as a reference and the charging effects were corrected according to that value.

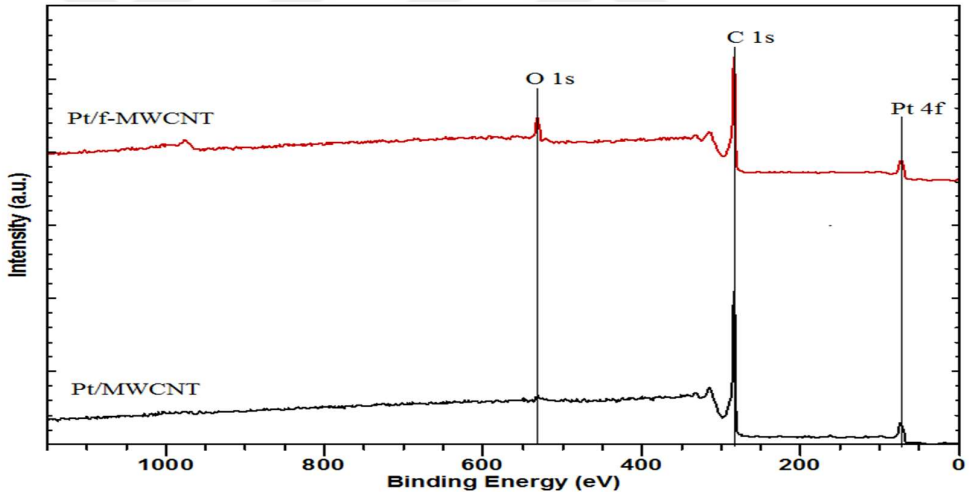

Figure 4.10. XPS spectrum for Pt/MWCNT 17 wt% and Pt/f-MWCNT 14 wt%

Pt 4f peak consists of two pairs of doublet ($4f_{7/2}$ and $4f_{5/2}$) with the spin orbit splitting of 3.33 eV. The relative intensity of the doublet peaks is 4:3 with equal half widths. These doublet peaks are relative to both Pt(0), Pt(II) and Pt(IV) with values of (71.1, 72.5, 74.4) and (74.9, 76.1, 78.2), respectively [65]. The ratio between Pt(0) to Pt(II+IV) was obtained from the area ratio of the fitted peaks. Figure 4.6 shows the XPS fitted peaks and Table 4.4 shows the position values of each peak plus the ratio of Pt(0) to Pt(IV) for each catalyst.

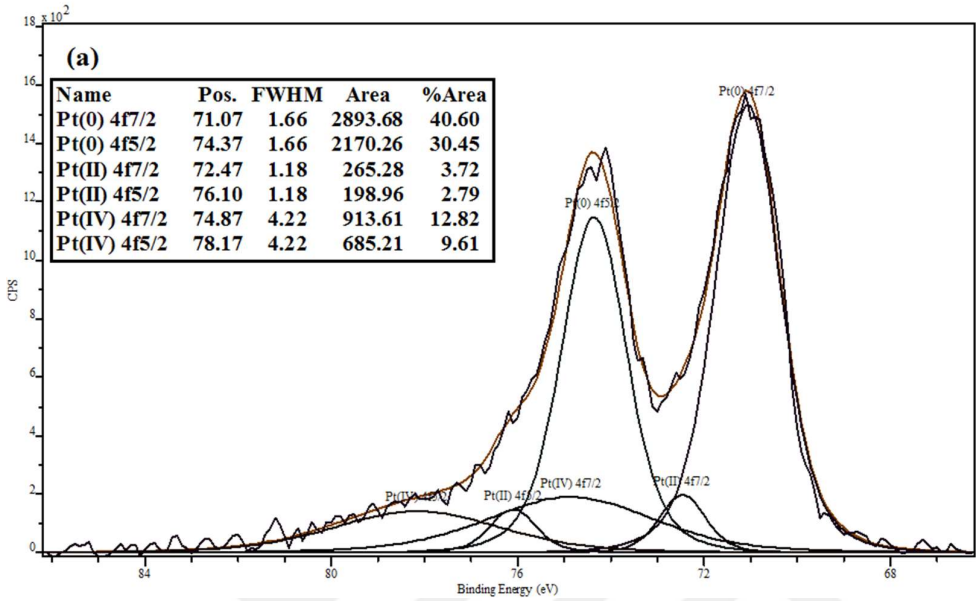
(a)
Name Pos. FWHM Area %Area
Pt(0) 4f7/2 71.07 1.66 2893.68 40.60
Pt(0) 4f5/2 74.37 1.66 2170.26 30.45
Pt(II) 4f7/2 72.47 1.18 265.28 3.72
Pt(II) 4f5/2 76.10 1.18 198.96 2.79
Pt(IV) 4f7/2 74.87 4.22 913.61 12.82
Pt(IV) 4f5/2 78.17 4.22 685.21 9.61
x 10^2
CPS
Binding Energy (eV)
Pt(0) 4f7/2
Pt(0) 4f5/2
Pt(IV) 4f7/2
Pt(II) 4f7/2

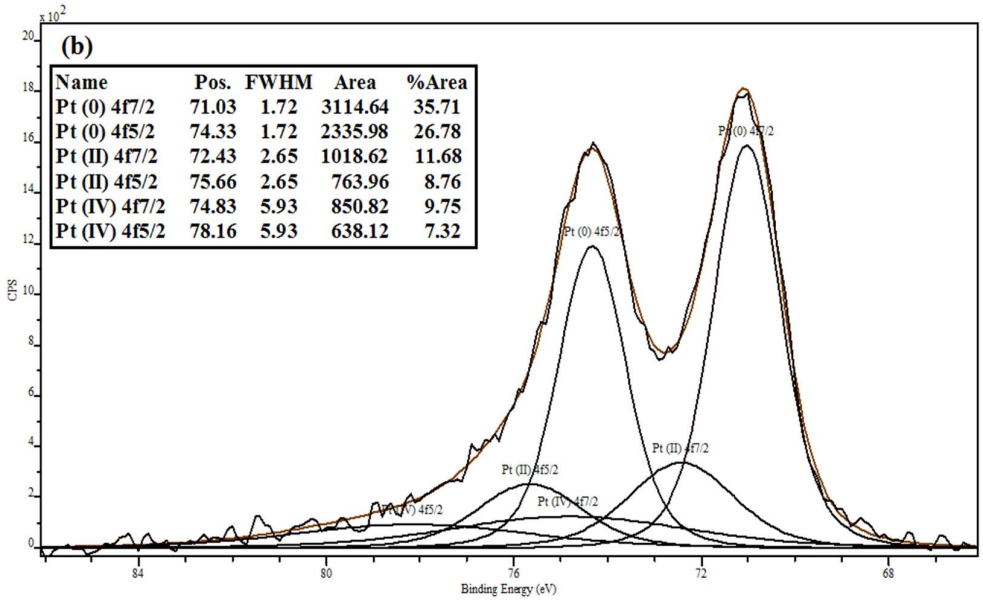
(b)
Name Pos. FWHM Area %Area
Pt (0) 4f7/2 71.03 1.72 3114.64 35.71
Pt (0) 4f5/2 74.33 1.72 2335.98 26.78
Pt (II) 4f7/2 72.43 2.65 1018.62 11.68
Pt (II) 4f5/2 75.66 2.65 763.96 8.76
Pt (IV) 4f7/2 74.83 5.93 850.82 9.75
Pt (IV) 4f5/2 78.16 5.93 638.12 7.32
x 10^2
CPS
Binding Energy (eV)
Pt (0) 4f7/2
Pt (0) 4f5/2
Pt (II) 4f7/2
Pt (II) 4f5/2
Pt (IV) 4f7/2

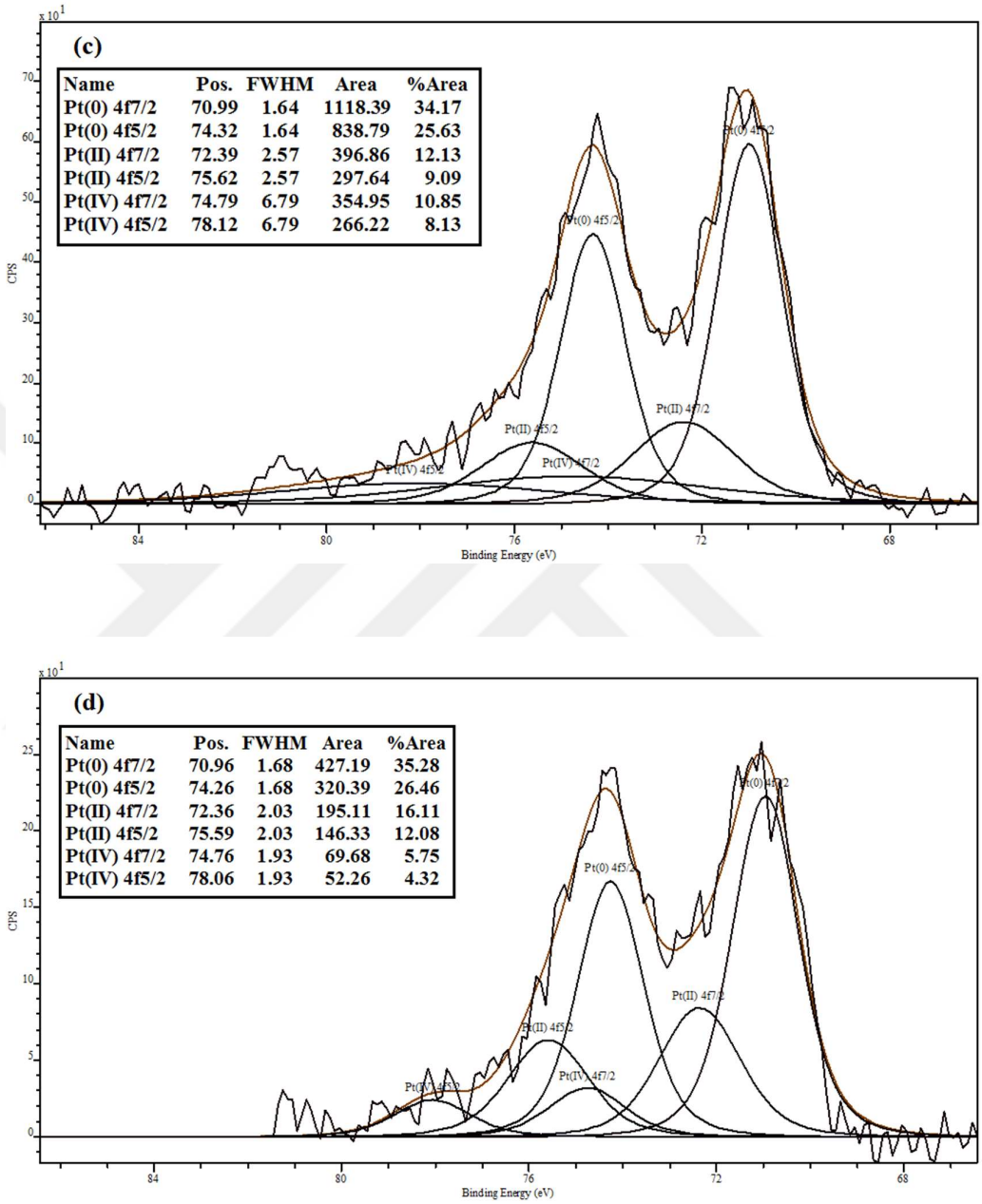

Figure 4.11. XPS peaks fitting for (a) Pt/MWCNT 17 wt%, (b) Pt/f-MWCNT 14 wt%, (c) Pt/f-MWCNT 10 wt%, (d) Pt/f-MWCNT 4 wt%

Table 4.5. Position values and ratio of Pt(0) to Pt(II+IV) for each catalyst

Catalyst	Pt(0)	Pt(II)	Pt(IV)	Ratio of Pt(0)/Pt(II+IV)
Pt/MWCNT 17 wt%	71.07 (71.05)	72.47 (6.51)	74.87 (22.43)	**2.45**
Pt/f-MWCNT 14 wt%	71.03 (62.49)	72.43 (20.44)	74.83 (17.07)	**1.67**
Pt/f-MWCNT 10 wt%	70.99 (59.8)	72.39 (21.22)	74.79 (18.98)	**1.48**
Pt/f-MWCNT 4 wt%	70.96 (61.74)	72.36 (28.19)	74.76 (10.07)	**1.62**

The highest oxidation state is for the Pt(0) ~ 65% followed by Pt(II) ~ 20% and Pt(IV) ~ 15%. This result indicate the good Pt(0) to Pt(II+IV) ratios which indicates the higher formation of the metallic Pt nanoparticles than the oxide formation.

4.2.5 Cyclic Voltammetry (CV)

To define the electrochemical properties and the activity of the catalysts toward methanol oxidation reaction, the cyclic voltammetry technique was used. The electrochemical surface area, the utility of the catalysts and the roughness factor values for each catalyst were calculated from the cyclic voltammograms.

In the case of the electrochemical analysis, voltage swept from -0.02V to 1.2V in acidic solution shows the hydrogen adsorption ($H_{ads.}$) and hydrogen desorption ($H_{des.}$) curves between -0.2 – 0.1 V which are shown in Figure 4.12. These curves are the result of the adsorption and desorption of the hydrogen atoms in the electrolyte on the surface of Pt nanoparticles.

The electro-oxidation of methanol on the synthesized Pt nanoparticles was analyzed by the two current peaks on the forward and reverse scan. In the forward scan, the peak is for the oxidation of the freshly adsorbed species of methanol. The methanol oxidation reaction starts at potentials around 0.3-0.4 V and reaches maximum potential at around 0.6-0.8 V. The reverse scan is the result of the removal of carbonaceous species which were not completely oxidized in the forward scan [66] as shown Figure 4.13. The amount of the peak maximum in the forward scan represent the activity of the synthesized catalyst for the electro-oxidation reaction of methanol.

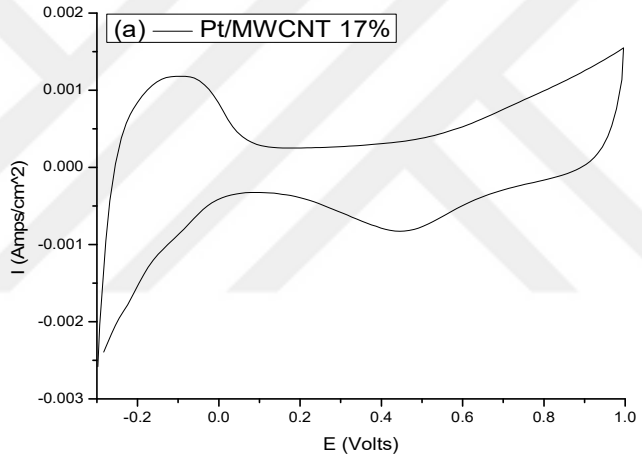

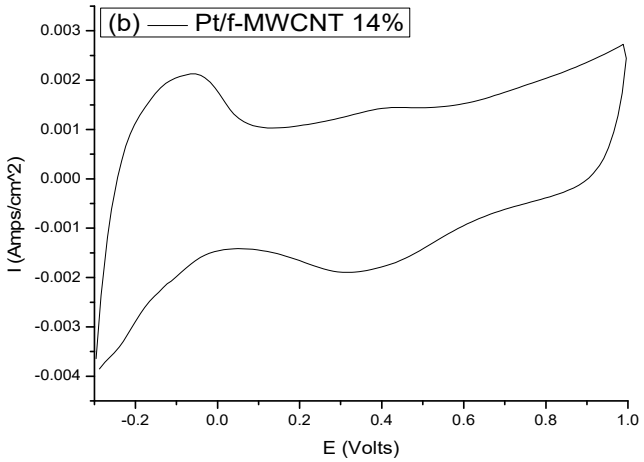

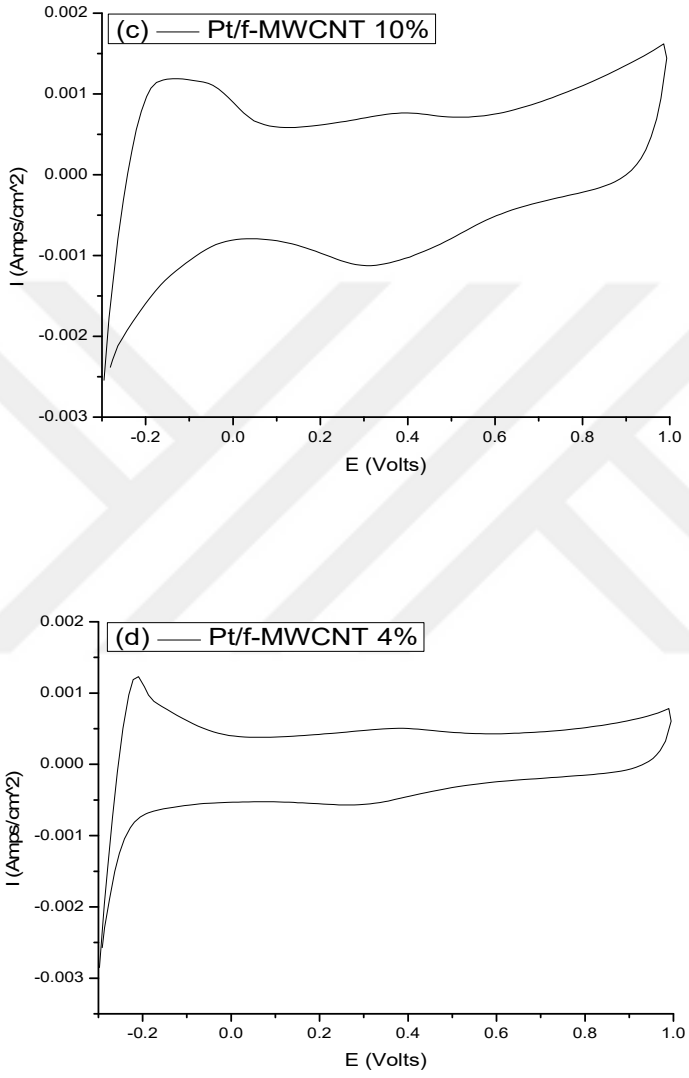

Figure 4.12. Cyclic voltammograms (-0.2 – 1.0 V) for (c) Pt/f-MWCNT 10 wt%, (d) Pt/f-MWCNT 4 wt% in 0.1 M $HClO_4$ at room temperature

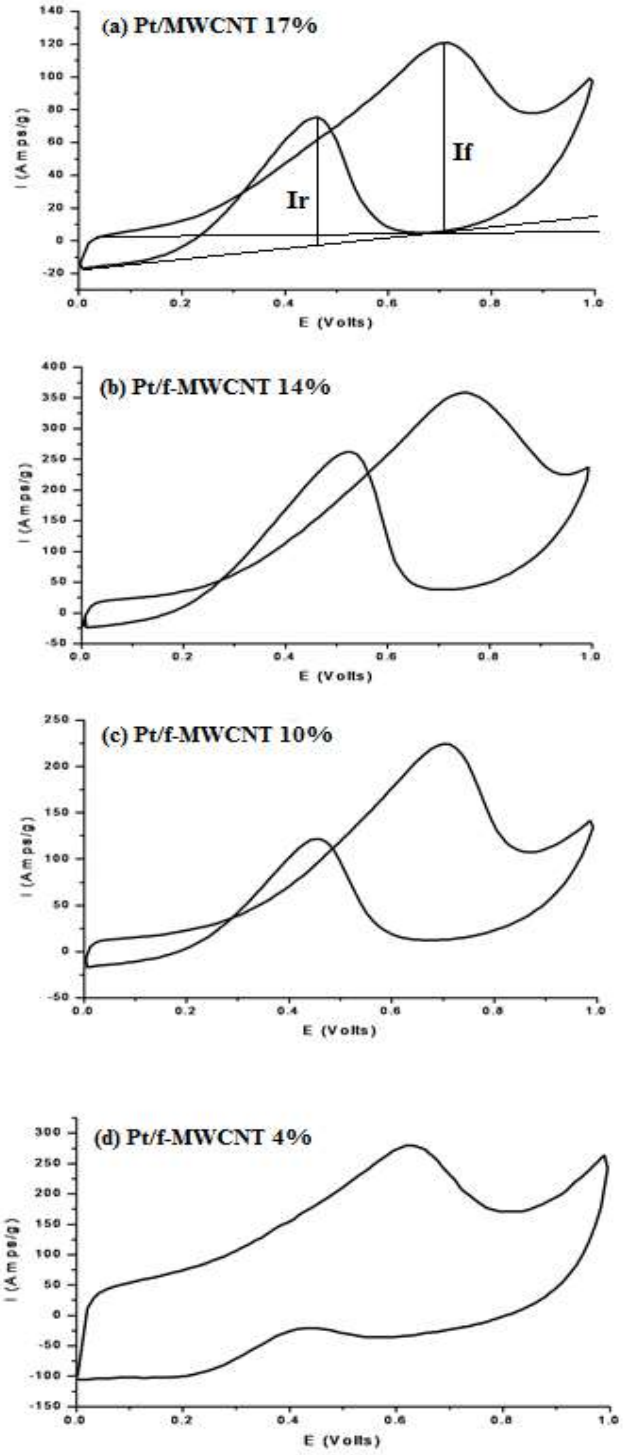

Figure 4.13. Cyclic voltammograms (0.0 – 1.0 V) for (a) Pt/MWCNT 17 wt%, (b) Pt/f-MWCNT 14 wt%, (c) Pt/f-MWCNT 10 wt%, (d) Pt/f-MWCNT 4 wt% in 0.1 M $HClO_4$ + 0.5 M CH_3OH at room temperature

The activity of the catalyst toward methanol oxidation reaction was investigated by CV measurements between 0.0 and 1.0 Volts in an electrochemical cell containing 0.1 M $HClO_4$ + 0.5 M CH_3OH electrolyte solution at room temperature with scan rate of 50 mV/s. The measurements were done with at least ten cycles for one working electrode and more than twenty different working electrodes were used for one catalyst sample.

Figure 4.13 shows the cyclic voltammograms for the four catalysts samples in 0.1 M $HClO_4$ + 0.5 M CH_3OH. The obtained activities for the Pt/MWCNT 17 wt%, Pt/f-MWCNT 14 wt%, Pt/f-MWCNT 10 wt% and Pt/f-MWCNT 4 wt%, were 120, 360 ,300 and 280 (Amps/g Pt) respectively. These values are listed in Table 4.6 with the value of the on-set potentials, the voltage maxima and the poisoning degrees (If/Ir) of all catalyst samples. For the comparison of their activities, the oxidation peaks of the four catalyst samples are also shown in Figure 4.14. The on-set potentials for the catalysts are almost the same between 0.25- 0.32 V. The poisoning degree is the ratio of the forward maximum current value (If) to the reverse maximum current value (Ir). This value indicates the degree for the catalyst to completely oxidize the adsorbed methanol molecules and the formed intermediates. Higher ratio indicates the complete oxidation of methanol with less formation of the intermediates on the surface of the Pt nanoparticles.

The highest activity for the methanol oxidation reaction was observed for Pt/f-MWCNT 14 wt% which can be related to the small particle size (2.79 nm) and the good size distribution of the Pt nanoparticles. At the same time, high activity results but lower than Pt/f-MWCNT 14% were obtained for the Pt/f-MWCNT 10 and 4 wt% attributable to the small particle sizes (2.70 and 2.57) and the size distribution. In the other hand, lower activity was recorded for the Pt/MWCNT 17 wt% sample which is the result of the low quality and the agglomeration of the formed nanoparticles.

The obtained activities were very high compared to the activity of the commercial catalysts and the Pt/MWCNT in the literature. The activity of the commercial catalyst

named as E-TEK 40% Pt/Vulcan XC-72 and Pt/MWCNT are 75 and 140 A/(g of Pt) respectively [66]. The activity of Pt/f-MWCNT 14% is 4.8 times active than the commercial catalyst E-TEK 40% Pt/Vulcan XC-72 and 2.5 than the Pt/MWCNT.

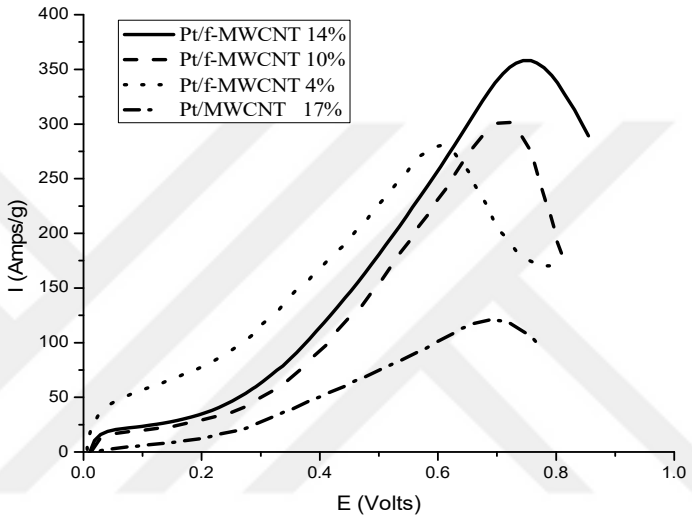

Figure 4.14. Methanol oxidation peaks for all catalytic samples

Table 4.6. Activity (potential and current) maxima and poisoning degrees for the catalyst samples

Catalyst	On-set potential (Volts)	V max (volts)	I max (Amps/g)	If/Ir
Pt/CNT 17%	0.25	0.71	120	1.3
Pt/f-CNT 14%	0.30	0.75	360	1.2
Pt/f-CNT 10%	0.32	0.70	300	1.7
Pt/f-CNT 4%	0.25	0.63	280	2.6

The electrochemical properties of the synthesized catalysts were investigated by finding the percent utility of the catalyst, the chemical surface area (CSA), the electrochemical surface area (ECSA), and the roughness factor.

The CSA is the direct surface area of the catalyst that is calculated from the average particle size of the catalyst. The CSA of the catalyst samples were calculated using the following equation:

$$CSA = \frac{6000}{\rho\, d}$$

Where **ρ** is the density of Pt metal (21.40 g/cm^3), and **d** is the crystalline particle diameter in (nm) obtained from TEM characterization [67]. The values of the calculated CSAs are found in Table 4.7.

The ECSA represents the active sites on the surface of the catalyst toward methanol oxidation reaction. The calculation of ECSA of each catalyst sample from the charge values and quantities of platinum was performed using the following equation:

$$ECA = \frac{Q_H}{0.21 \times [Pt]}$$

where Q_H is the electrical charge for hydrogen adsorption in (mC), 0.21 (in mC/cm^2) is the Pt crystalline activity surface area transition constant and [Pt] (in mg/cm^2) is the Pt loading on the used electrodes calculated from ICP-MS results [67].

The charge values were obtained from CV voltammograms in the range of -0.2 to 1.2 V in 0.1 M $HClO_4$ at room temperature Figure 4.13. The charge values were calculated by integration of the area under the hydrogen adsorption peak. The charge values and the calculated CSA and ECSA values of the catalysts are listed in Table 4.7.

From the CSA and the ECSA, the Pt utilization % can be calculated using:

$$Utilization\% = \frac{ECSA}{CSA} \times 100$$

Table 4.7. Chemical and electrochemical surface areas, charges, and percent utility of the catalyst samples

Catalyst	Amount (g/cm2)	Size (nm)	CSA (m^2/g)	Charge (mcoul)	ECSA (m^2/g)	% Utility
Pt/CNT 17 wt%	8.55325×10^{-5}	1.95	**143.78**	**6.17**	**34.35**	**24.0**
Pt/f-CNT 14 wt %	7.09351×10^{-5}	2.74	**102.33**	**10.77**	**72.30**	**70.9**
Pt/f-CNT 10 wt %	5.08052×10^{-5}	2.70	**103.84**	**6.32**	**59.24**	**57.3**
Pt/f-CNT 4 wt %	1.89091×10^{-5}	2.57	**109.09**	**2.56**	**64.47**	**59.4**

The values obtained from the electrochemical analysis are compatible with the high activity results of the Pt/f-MWCNT 14 wt% in methanol oxidation reaction. The ECSA is the highest for Pt/f-MWCNT 14 wt% with 72.30 m^2/g and %utility of 70.9. The ESCA values and the %utility of the other Pt/f-MWCNT catalysts are 64.47 and 59.4%, 59.24 and 57.3% for Pt/f-MWCNT 4 wt% and Pt/f-MWCNT 10 wt%, respectively. The lowest ECSA and %utility was recorded for Pt/MWCNT 17 wt% with 34.35 m^2/g and 24%. These low values which are also related to the low activity in methanol oxidation reaction for Pt/MWCNT 17 wt% catalyst is due to the agglomeration of the Pt nanoparticles.

The roughness factors for the catalyst samples were also calculated from the ratio of the real area (A_{real}) over the geometrical area ($A_{geom.}$);

$$R.F. = \frac{A(real.)}{A(geom.)}$$

where, the ($A_{geom.}$) geometrical area is the area of the electrode used for the measurements with radius of 0.35 cm and area value of 0.38 cm^2 since $A = \pi r^2$.

The real area can be calculated by the following equation;

$$A(real.) = \frac{Q}{0.21}$$

where, (Q) is the charge value in (mC) and the coefficient 0.21 in (mC/cm^2) [68]. The obtained roughness factor values are summarized in table 4.8.

Table 4.8. Charge, real area and roughness factor values

Catalyst	Charge (mC)	A_{real} (cm^2)	Roughness Factor
Pt/CNT 17 wt%	6.17	29.38	77.12
Pt/f-CNT 14 wt%	10.77	51.28	134.96
Pt/f-CNT 10 wt%	6.32	30.09	79.20
Pt/f-CNT 4 wt%	2.56	12.19	32.08

As can be seen from the Table 4.8, the highest roughness factor value is for the Pt/f-MWCNT 14 wt% with 134.96 which is compatible with its high activity in methanol

oxidation reaction and %utility. The reason for the high activity is in the small particle size and the good size distribution which increase the number of active sites on the catalyst. The obtained high roughness factor values can be also related to the unique network nano-structure of the MWCNT [69] which effectively increase the number of the active sites in the catalyst.

CHAPTER 5

CONCLUSION

MWCNT and f-MWCNT supported Pt nanoparticles were prepared with impregnation method and hydrogen gas reduction. The synthesized nanoparticles were used as electro-catalysts for the methanol oxidation reaction. Four catalyst samples were successfully synthesized and tested for the methanol oxidation reaction. These samples are Pt/MWCNT 17wt% and Pt/f-MWCNT 14, 10, and 4 wt%. For the Pt/f-MWCNT catalyst samples, the functionalization of MWCNT was achieved by oxidation in strong acidic solution using sonochemical method. The functional groups were studied using FTIR and XPS techniques and the results showed the formation of oxygen containing groups of carboxyl, carbonyl and hydroxyl.

TEM images and XRD patterns revealed the average particle size to be 2.5 nm. Pt/f-MWCNT had larger Pt nanoparticles and small range of size distribution than the Pt/MWCNT samples. Moreover, agglomeration of the Pt nanoparticles were observed in the Pt/MWCNT samples. The results specify the importance of the functional groups in the formation of the Pt nanoparticles. The functional groups improved the dispersion of the precursor over the f-MWCNT by increasing the uniform adsorption of the precursor on the surface of the MWCNT.

XPS results revealed the presence of two oxidation states Pt(0) and Pt(IV). The Pt(0) to Pt(IV) oxidation state ratio for all catalysts were above 3.0 which indicates the excellent formation of the zero state Pt nanoparticles.

The highest activity was recorded for the Pt/f-MWCNT 14 wt% catalyst sample at 360 A/g which is 4.8 times higher than the commercial catalyst E-TEK 40% Pt/Vulcan XC-72 with 75A/g. This is due to its high electrochemical surface area (72.3 m^2/g), %Pt utility (70.9%) and roughness factor (134.96) values. The lowest ECSA value and %utility was for Pt/MWCNT 17% sample with 34.35 m^2/g and 24 utility%. The low values are due to the agglomeration of the Pt nanoparticles in the Pt/MWCNT 17 wt% catalyst.

The obtained results also show the simplicity and efficiency of the used impregnation method in the preparation of the f-MWCNT supported Pt nanoparticles with small and acceptable Pt nanoparticles size distribution because of the unique nano-structure of the f-MWCNT acts as a templet for the Pt nanoparticles.

REFERENCES

[1] I. EG&G Technical Services, "Fuel Cell Handbook," *Fuel Cell*, vol. 7 Edition, no. November, pp. 1–352, 2004.

[2] M. P. Hogarth and G. A. Hards, "Direct Methanol Fuel Cells," *Platin. Met. Rev.*, vol. 40, no. 1, pp. 150–159, 1996.

[3] M. S. Larminie, J., Dicks, A., McDonald, *Fuel cell systems explained*, vol. 2. 2003.

[4] M. Winter and R. J. Brodd, "What are batteries, fuel cells, and supercapacitors?," *Chem. Rev.*, vol. 104, no. 10, pp. 4245–4269, 2004.

[5] H. A. Gasteiger, D. R. Baker, R. N. Carter, W. Gu, Y. Liu, F. T. Wagner, and P. T. Yu, "Electrocatalysis and Catalyst Degradation Challenges in Proton Exchange Membrane Fuel Cells," *Hydrog. Energy*, pp. 3–16, 2010.

[6] X. Li, *Principles of fuel cells*. 2006.

[7] H. J. Schwartz, *Fuel cells - From Fundamentals to Applications*. 2006.

[8] J. M. Andújar and F. Segura, "Fuel cells: History and updating. A walk along two centuries," *Renew. Sustain. Energy Rev.*, vol. 13, no. 9, pp. 2309–2322, Dec. 2009.

[9] C. Rayment and S. Sherwin, *Introduction to Fuel Cell Technology*. 2003.

[10] Fuel Cell Today, "'The Fuel Cell Industry Review 2012,'" 2012.

[11] X. Li, *Chapter One Thermodynamic Performance of Fuel Cells and Comparison with Heat Engines*, vol. 1. 2007.

[12] L. Carrette, K. A. Friedrich, and U. Stimming, "Fuel Cells: Principles, Types, Fuels, and Applications," *ChemPhysChem*, vol. 1, no. 4, pp. 162–193, 2000.

[13] A. J. Appleby and F. R. Foulkes, "Fuel Cell Handbook," 1989.

[14] P. Joghee, J. N. Malik, S. Pylypenko, and R. O'Hayre, "A review on direct methanol fuel cells – In the perspective of energy and sustainability," *MRS Energy Sustain.*, vol. 2, pp. 1–31, 2015.

[15] IEA-ETSAP and IRENA, "Production of Bio-methanol - Technology Brief," 2013.

[16] A. S. Aricò, S. Srinivasan, and V. Antonucci, "DMFCs: From Fundamental Aspects to Technology Development," *Fuel Cells*, vol. 1, no. 2, pp. 133–161, 2001.

[17] T. Iwasita, "Electrocatalysis of methanol oxidation," *Electrochim. Acta*, vol. 47, no. 22–23, pp. 3663–3674, 2002.

[18] H. Lei, P. Atanassova, Y. Sun, and B. Blizanac, "State-of-the-Art Electrocatalysts for Direct Methanol Fuel Cells," in *Electrocatalysis of Direct Methanol Fuel Cells: From Fundamentals to Applications*, 2009, pp. 197–226.

[19] F. Şen, "The Preparation and Analysis of New Carbon Supported Pt and Pt+Second Metal Nanoparticles Catalysts for Direct Methanol Fuel Cells," *Dr. Philos. Thesis Chem. METU, ANKARA*, 2013.

[20] N. C. Bagkar, H. M. Chen, H. Parab, and R. S. Liu, "Nanostructured Electrocatalyst Synthesis: Fundamental and Methods," *Electrocatal. Direct*

Methanol Fuel Cells From Fundam. to Appl., pp. 79–114, 2009.

[21] H. Liu, C. Song, L. Zhang, J. Zhang, H. Wang, and D. P. Wilkinson, "A review of anode catalysis in the direct methanol fuel cell," *J. Power Sources*, vol. 155, no. 2, pp. 95–110, 2006.

[22] M. Yaldagard, "Carbonaceous Nanostructured Support Materials for Low Temperature Fuel Cell Electrocatalysts—A Review," *World J. Nano*, vol. 2013, no. December, pp. 121–153, 2013.

[23] E. T. Thostenson, Z. Ren, and T.-W. Chou, "Advances in the science and technology of carbon nanotubes and their composites: a review," *Compos. Sci. Technol.*, vol. 61, no. 13, pp. 1899–1912, 2001.

[24] A. Peigney, C. Laurent, E. Flahaut, R. R. Bacsa, and A. Rousset, "Specific surface area of carbon nanotubes and bundles of carbon nanotubes," *Carbon N. Y.*, vol. 39, no. 4, pp. 507–514, 2001.

[25] V. Choudhary and A. Gupta, "Polymer / Carbon Nanotube Nanocomposites," *Intech*, pp. 65–90, 2001.

[26] B. Scheibe, E. Borowiak-Palen, and R. J. Kalenczuk, "Oxidation and reduction of multiwalled carbon nanotubes — preparation and characterization," *Mater. Charact.*, vol. 61, no. 2, pp. 185–191, Feb. 2010.

[27] K. Balasubramanian and M. Burghard, "Chemically functionalized carbon nanotubes," *Small*, vol. 1, no. 2, pp. 180–192, 2005.

[28] B. Xue, P. Chen, Q. Hong, J. Lin, and K. L. Tan, "Growth of Pd, Pt, Ag and Au nanoparticles on carbon nanotubes," *J. Mater. Chem.*, 2001.

[29] N. Job, M. F. R. Pereira, S. Lambert, A. Cabiac, G. Delahay, J. F. Colomer, J.

Marien, J. L. Figueiredo, and J. P. Pirard, “Highly dispersed platinum catalysts prepared by impregnation of texture-tailored carbon xerogels,” *J. Catal.*, vol. 240, no. 2, pp. 160–171, 2006.

[30] L. B. Okhlopkova, “Properties of Pt/C catalysts prepared by adsorption of anionic precursor and reduction with hydrogen. Influence of acidity of solution,” *Appl. Catal. A Gen.*, vol. 355, no. 1–2, pp. 115–122, 2009.

[31] S. Lambert, N. Job, L. D’Souza, M. F. R. Pereira, R. Pirard, B. Heinrichs, J. L. Figueiredo, J. P. Pirard, and J. R. Regalbuto, “Synthesis of very highly dispersed platinum catalysts supported on carbon xerogels by the strong electrostatic adsorption method,” *J. Catal.*, vol. 261, no. 1, pp. 23–33, 2009.

[32] V. S. Thoi, R. E. Usiskin, and S. M. Haile, “Platinum-decorated carbon nanotubes for hydrogen oxidation and proton reduction in solid acid electrochemical cells,” *Chem. Sci.*, vol. 6, pp. 1570–1577, 2015.

[33] Y. Xing, “Synthesis and electrochemical characterization of uniformly-dispersed high loading Pt nanoparticles on sonochemically-treated carbon nanotubes,” *J. Phys. Chem. B*, vol. 108, no. 50, pp. 19255–19259, 2004.

[34] S. Sharma and B. G. Pollet, “Support materials for PEMFC and DMFC electrocatalysts - A review,” *J. Power Sources*, vol. 208, pp. 96–119, 2012.

[35] Y. C. Chiang, W. H. Lin, and Y. C. Chang, “The influence of treatment duration on multi-walled carbon nanotubes functionalized by H2SO4/HNO3 oxidation,” *Appl. Surf. Sci.*, vol. 257, no. 6, pp. 2401–2410, Jan. 2011.

[36] A. B. González-Guerrero, E. Mendoza, E. Pellicer, F. Alsina, C. Fernández-Sánchez, and L. M. Lechuga, “Discriminating the carboxylic groups from the total acidic sites in oxidized multi-wall carbon nanotubes by means of acid-base titration,” *Chem. Phys. Lett.*, vol. 462, no. 4–6, pp. 256–259, 2008.

[37] M. A. Ganzoury, N. K. Allam, T. Nicolet, and C. All, “Introduction to Fourier Transform Infrared Spectrometry,” *Renew. Sustain. Energy Rev.*, vol. 50, pp. 1–8, 2015.

[38] S. Hofmann, *Auger- and X-Ray Photoelectron Spectroscopy in Materials Science*. 2013.

[39] J. F. Watts and J. Wolstenholme, *An Introduction to Surface Analysis by XPS and AES*. 2015.

[40] H. Hu, P. Bhowmik, B. Zhao, M. . Hamon, M. . Itkis, and R. . Haddon, “Determination of the acidic sites of purified single-walled carbon nanotubes by acid–base titration,” *Chem. Phys. Lett.*, vol. 345, no. 1–2, pp. 25–28, Sep. 2001.

[41] V. S. Thoi, R. E. Usiskin, and S. M. Haile, “Platinum-decorated carbon nanotubes for hydrogen oxidation and proton reduction in solid acid electrochemical cells,” *Chem. Sci.*, vol. 6, pp. 1570–1577, 2015.

[42] G. Gökağaç, J. M. Léger, and F. Hahn, “Behaviour of bimetallic Pt-Pd carbon-supported catalysts in methanol electrooxidation,” *Zeitschrift fur Naturforsch. - Sect. B J. Chem. Sci.*, vol. 58, no. 5, pp. 423–432, 2003.

[43] Y. Waseda, E. Matsubara, and K. Shinoda, *X-Ray Diffraction Crystallography*. 2011.

[44] Y. Leng, *Materials characterization:Introduction to Microscopic and Spectroscopic materials*, Second Edi. 2009.

[45] C. Stadtländer, “Scanning electron microscopy and transmission electron microscopy of mollicutes: challenges and opportunities,” in *Modern Research and Educational Topics in Microscopy*, 2007, pp. 122–131.

[46] D. B. Williams and C. B. Carter, *Transmission Electron Microscopy: A Textbook for Materials Science*. 2009.

[47] R. Thomas, *Practical Guide to ICP-MS*. 2004.

[48] C. Brett and A. Brett, *Electrochemistry: principles, methods, and applications*. 1993.

[49] S. P. Kounaves, "Voltammetric Techniques," in *Handbook of Instrumental Techniques for Analytical Chemistry*, 2015, pp. 709–725.

[50] V. Datsyuk, M. Kalyva, K. Papagelis, J. Parthenios, D. Tasis, A. Siokou, I. Kallitsis, and C. Galiotis, "Chemical oxidation of multiwalled carbon nanotubes," *Carbon N. Y.*, vol. 46, no. 6, pp. 833–840, May 2008.

[51] K. A. Wepasnick, B. A. Smith, K. E. Schrote, H. K. Wilson, S. R. Diegelmann, and D. H. Fairbrother, "Surface and structural characterization of multi-walled carbon nanotubes following different oxidative treatments," *Carbon N. Y.*, vol. 49, no. 1, pp. 24–36, Jan. 2011.

[52] B. H. Stuart, *Infrared Spectroscopy: Fundamentals and Applications*. 2005.

[53] L. Stobinski, B. Lesiak, L. Kövér, J. Tóth, S. Biniak, G. Trykowski, and J. Judek, "Multiwall carbon nanotubes purification and oxidation by nitric acid studied by the FTIR and electron spectroscopy methods," *J. Alloys Compd.*, vol. 501, no. 1, pp. 77–84, Jul. 2010.

[54] F. Avilés, J. V. Cauich-Rodríguez, L. Moo-Tah, A. May-Pat, and R. Vargas-Coronado, "Evaluation of mild acid oxidation treatments for MWCNT functionalization," *Carbon N. Y.*, vol. 47, no. 13, pp. 2970–2975, 2009.

[55] J. Coates, "Interpretation of Infrared Spectra, A Practical Approach," *Encycl.*

Anal. Chem., pp. 10815–10837, 2000.

[56] S. M. Yun, J. W. Kim, M. J. Jung, Y. C. Nho, P. H. Kang, and Y. S. Lee, "An XPS Study of Oxyfluorinated Multiwalled Carbon Nano Tubes," *Carbon Lett.*, vol. 8, no. 4, pp. 292–298, 2007.

[57] W. Xia, Y. Wang, R. Bergsträßer, S. Kundu, and M. Muhler, "Surface characterization of oxygen-functionalized multi-walled carbon nanotubes by high-resolution X-ray photoelectron spectroscopy and temperature-programmed desorption," *Appl. Surf. Sci.*, vol. 254, no. 1 SPEC. ISS., pp. 247–250, 2007.

[58] A. P. Terzyk, M. Wiśniewski, P. A. Gauden, G. Rychlicki, and S. Furmaniak, "Carbon surface chemical composition in para-nitrophenol adsorption determined under real oxic and anoxic conditions," *J. Colloid Interface Sci.*, vol. 320, no. 1, pp. 40–51, 2008.

[59] M. Wahlqvist and A. Shchukarev, "XPS spectra and electronic structure of Group IA sulfates," *J. Electron Spectros. Relat. Phenomena*, vol. 156–158, no. May 2007, pp. 310–314, 2007.

[60] K. A. Wepasnick, B. A. Smith, J. L. Bitter, and D. Howard Fairbrother, "Chemical and structural characterization of carbon nanotube surfaces," *Anal. Bioanal. Chem.*, vol. 396, no. 3, pp. 1003–1014, 2010.

[61] S. Horikoshi and N. Serpone, "Introduction to Nanoparticles," *Microwaves Nanoparticle Synth. Fundam. Appl.*, pp. 1–24, 2013.

[62] R. Singh, R. Awasthi, and C. Sharma, "Review : An Overview of Recent Development of Platinum- Based Cathode Materials for Direct Methanol Fuel Cells," *Int. J. Electrochem. Sci*, vol. 9, pp. 5607–5639, 2014.

[63] X. Yu and S. Ye, “Recent advances in activity and durability enhancement of Pt/C catalytic cathode in PEMFC. Part I. Physico-chemical and electronic interaction between Pt and carbon support, and activity enhancement of Pt/C catalyst,” *J. Power Sources*, vol. 172, no. 1, pp. 133–144, 2007.

[64] J. Schindelin, I. Arganda-Carreras, E. Frise, V. Kaynig, M. Longair, T. Pietzsch, S. Preibisch, C. Rueden, S. Saalfeld, B. Schmid, J.-Y. Tinevez, D. J. White, V. Hartenstein, K. Eliceiri, P. Tomancak, and A. Cardona, “Fiji: an open-source platform for biological-image analysis,” *Nat. Methods*, vol. 9, no. 7, pp. 676–682, 2012.

[65] Z. Ozturk, F. Sen, S. Sen, and G. Gokagac, “The preparation and characterization of nano-sized Pt-Pd/C catalysts and comparison of their superior catalytic activities for methanol and ethanol oxidation,” *J. Mater. Sci.*, vol. 47, no. 23, pp. 8134–8144, 2012.

[66] F. Şen and G. Gökagaç, “Activity of carbon-supported platinum nanoparticles toward methanol oxidation reaction: Role of metal precursor and a new surfactant, tert-octanethiol,” *J. Phys. Chem. C*, vol. 111, no. 3, pp. 1467–1473, 2007.

[67] B. Krishnamurthy and S. Deepalochani, “Performance of Platinum Black and Supported Platinum Catalysts in a Direct Methanol Fuel Cell,” *Int. J. Electrochem. Sci*, vol. 4, pp. 386–395, 2009.

[68] Z. Dongping, J. Velmurugan, and M. V. Mirkin, “Adsorption/desorption of hydrogen on Pt nanoelectrodes: Evidence of surface diffusion and spillover,” *J. Am. Chem. Soc.*, vol. 131, no. 41, pp. 14756–14760, 2009.

[69] D. Tasis, N. Tagmatarchis, A. Bianco, and M. Prato, “Chemistry of carbon nanotubes,” *Chem. Rev.*, vol. 106, no. 3, pp. 1105–1136, 2006.